Copyright © 1999, by the author(s).
All rights reserved.

Permission to make digital or hard copies of all or part of this work for personal or classroom use is granted without fee provided that copies are not made or distributed for profit or commercial advantage and that copies bear this notice and the full citation on the first page. To copy otherwise, to republish, to post on servers or to redistribute to lists, requires prior specific permission.

MOVING BOUNDARY MODELS AND METHODS FOR DEEP SUBMICRON RESIST PROCESS SIMULATION

by

Ebo Croffie

Memorandum No. UCB/ERL M99/26

20 May 1999

MOVING BOUNDARY MODELS AND METHODS FOR DEEP SUBMICRON RESIST PROCESS SIMULATION

by

Ebo Croffie

Memorandum No. UCB/ERL M99/26

20 May 1999

ELECTRONICS RESEARCH LABORATORY

College of Engineering
University of California, Berkeley
94720

Moving Boundary Models and Methods for Deep Submicron Resist Process Simulation

Ebo Croffie

Memorandum No. UCB/ERL M99/26

May 20, 1999

Electronics Research Laboratory
College of Engineering
University of California, Berkeley

Moving Boundary Models and Methods for Deep Submicron Resist Process Simulation

by Ebo H. Croffie

Research Project

Submitted to the Applied Science and Technology Graduate Group, University of California at Berkeley, in partial satisfaction of the requirements for the degree of **Master of Science, Plan II.**

Approval for the Report and Comprehensive Examination:

Committee:

Professor
Research Advisor

May 20, 1999

(Date)

****

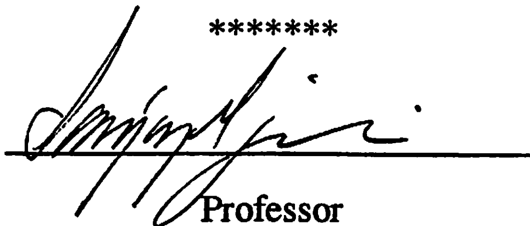

Professor
Second Reader

5/20/99

(Date)

Abstract

Moving Boundary Models and Methods for Deep Submicron Resist Process Simulation

by

Ebo Croffie

University of California at Berkeley

Professor Andrew R. Neureuther, Research Advisor

A new TCAD software tool named STORM (Simulation Tools for Optical Resist Models) has been developed to support the quantitative modeling of optical resist processes in deep submicron lithography. These processes such as post exposure bake (PEB) and silylation involve changing topographies and moving interfaces. Thus, accurate modeling has to take into account the sharp interface propagation and polymer deformation induced stress effects. Analytic solutions are not available for the model-equations and numerical algorithms have to be developed to simulate the physical models. This need for rigorous numerical methods to facilitate rapid simulation of optical resist processes has been the motivation for the development of STORM. Several numerical tools have been included in STORM to provide a general numerical framework for tackling complex model-equations encountered in optical lithography process modeling. STORM utilizes the finite element method to emulate the polymer deformation. For the sake of rapid simulation, we employ efficient numerical algorithms based on the second order backward difference formula (BDF2) and Krylov subspace methods in STORM. An order of magnitude increase in performance is achieved over classical numerical methods such as Crank-Nicolson method. Monte Carlo methods for simulating oxygen reactive ion etching for surface imaged resist processes are also employed in STORM.

The efficiency and flexibility of STORM at simulating highly nonlinear partial differential equations allows for the accuracy of moving boundary models to be explored. Thus, moving boundary models for PEB, silylation, wet development and dry development of surface imaged resists are chosen as test vehicles for STORM. Applications of these first pass models to deep submicron resist processes such as bilayer resist (BLR), top surface imaging (TSI) and chemically amplified resist (CAR) are demonstrated in this report. Simulation demonstration of special technology issues in 193nm lithography such as line end shortening (LES) in DUV resist and line edge roughness (LER) in surface imaged resist processes are also presented in this report. Simulation times for the highly stiff model-equations were less than 15 minutes except the dry development process, which took about an hour on a DEC Alpha 600 MHz machine. STORM program release information can be obtained at the following web site, http://microlab.eecs.berkeley.edu/~ebo.

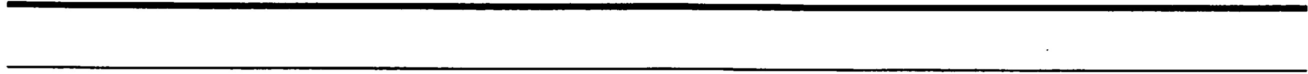

Acknowledgments

I would like to thank Professor Andrew R. Neureuther at the University of California at Berkeley and Professor Grant Willson at the University of Texas, Austin for their guidance. I would also like to thank my colleagues and friends, Mr. Shafiul Litu, Mr. Ibna Faruque, Mr. Mosong Cheng, Mr. Yashesh Shroff, Dr. Marco Zuniga, Dr. Fang Piao, Dr. Zulu Xaba, Professor Luke Lee and Professor Elinor Velasquez for their friendship and support.

This research was supported in part by the Semiconductor Research Corporation (95-LC-712-MC500), the SRC/DARPA Lithography Network (SRC 96-LL6-460/MDA 972-97-1-0010) and the California SMART program. Thanks to the University of California Graduate Division for granting me the Graduate Opportunity Program Fellowship (1996-1998).

Hi Mom ...

Table of Contents

Abstract v

Acknowledgments vii

Table of Contents ix

CHAPTER 1 Introduction 13

CHAPTER 2 Numerical Algorithms 15

2.1 Finite Element Space Discretization 15
2.1.1 Polymer linear viscoelastic model 17
2.1.2 Discretization of the linear momentum balance equation 18

2.2 BDF2 Time Discretization 20
2.2.1 Predictor for the initial Newton guess 20
2.2.2 The modified Newton method for BDF2 21
2.2.3 The Krylov subspace Newton convergence accelerator 21
2.2.4 The starting procedure 21

CHAPTER 3 Modeling Post Exposure Bake 23

3.1 Introduction 23

3.2 Moving Boundary Model for PEB 24
3.2.1 Diffusivity model 25
3.2.2 Reaction Rate model 26
3.2.3 Polymer relaxation 26
3.2.4 PEB diffusion/reaction kinetics 26
3.2.5 Differential Equations 27
3.2.6 Boundary conditions 27

3.3 Simplified PEB Models 27

CHAPTER 4 Modeling Silylation 31

4.1 Introduction 31
4.2 Moving Boundary Model for Silylation 33
4.2.1 Adsorption rate model 34
4.2.2 Diffusivity model 34
4.2.3 Polymer relaxation 35
4.2.4 Silylation diffusion/reaction kinetics 35
4.2.5 Differential Equations 35
4.2.6 Boundary conditions 36

CHAPTER 5 Modeling Wet Development 37

5.1 Introduction 37
5.2 Adsorption rate model 38
5.3 Diffusivity model 39
5.4 Wet development diffusion/reaction kinetics 39
5.5 Differential Equations 39
5.6 Boundary conditions 40

CHAPTER 6 Modeling O_2 Reactive Ion Etching for Surface Imaged Resists 41

6.1 Introduction 41
6.2 O_2 RIE plasma etching model for surfaced imaged resists 43
6.3 Monte-Carlo method for Ion bombardment 43
6.4 Dry development diffusion/reaction kinetics 44
6.5 Diffusivity model 44
6.6 Differential Equations 44
6.7 Boundary conditions 45

CHAPTER 7 Applications of STORM 47

7.1 Post exposure bake simulation 47
7.1.1 1D full model simulation results 44
7.1.2 2D MBT model (simplified) simulation results 49
7.1.3 2D Case II diffusion model simulation results 49
7.2 Silylation simulation 49
7.2.1 Positive tone diffusion enhanced silylation scheme 52
7.2.2 Negative tone non-diffusion enhanced silylation scheme 52
7.3 Wet development simulation 53
7.4 Dry development simulation 54
7.4.1 2D simulation results 56

7.5 193nm lithography applications **57**

7.5.1 193nm Chemically amplified resists 57
7.5.2 Top surface imaging (TSI) 58
7.5.3 Bilayer resist (BLR) 58

7.6 193nm lithography technology issues simulation **59**

7.6.1 Line edge roughness in surface imaged resist processes 60
7.6.2 Line-end shortening effects in DUV resist processes 61

CHAPTER 8 Summary **63**

References 65

CHAPTER 1 Introduction

Modeling and simulation of semiconductor processes are especially useful in coping with the complexity associated with today's advanced lithography processes and emerging technologies for tomorrow [1]. As new optical lithography exposure tools and resist materials for deep submicron applications emerge, accurate models and simulators for these processes become indispensable tools for understanding and optimizing the processes. At each change in wavelength, there is a renewed interest in surface imaged resist processes such as top surface imaging (TSI) and bilayer resists (BLR) since these processes offer viable extensions of current optical lithography tools for future generation integrated circuits (ICs). Modeling and simulation is useful for understanding factors responsible for various issues associated with the implementation of surface imaged systems for IC manufacturing and can provide directions for optimizing these processes.

A rigorous and flexible numerical framework for simulating resist mechanisms is needed for reliable prediction of resist profiles. A simulation program that provides such a framework has been developed and named STORM, which stands for Simulation Tools for Optical Resist Models.

The development of STORM is motivated by the need to support quantitative modeling of 193nm and EUV lithography processes such as BLR, TSI and chemically-amplified resist (CAR). These applications require simulation tools for post exposure bake (PEB), silylation, wet development and O_2 reactive ion etching (RIE) of surface imaged resists. First pass models for these processes are presented. The model-verification step requires systematic experimental data that can be readily quantified. The design of experimental procedure, calibration of the proposed models and future extensions of the algorithms will be the subject of the Ph.D. thesis.

The modeling efforts for resist processes were initiated by Dill et al [4]. This model was employed in developing the SAMPLE simulator [5]. Ferguson et al [6] proposed the first model for the CAR PEB process. Zuniga et al [3] and Mack [7] employed variations of this PEB model in developing a PEB process simulator.

For the TSI process, Hartney et al [8] presented a first pass model based on aerial image calculations. Pierret [9] proposed a mechanistic based model for the silylation process. Zuniga et al [10] extended this model to take into account possible stress accumulation during the silylation process.

The model-equations of the resist processes presented in this report take on the form of partial differential equations (PDEs). An approach suitable for solving the equations is to develop a semi-discrete analogue of the PDEs where the PDEs are discretized in space using the Finite Element Method (FEM) [14]. This consists of a discretization of a domain of interest, into elements with discrete endpoints, or nodes. The space discretization results in a system of stiff ordinary differential equations (ODEs) with the system size proportional to the number of nodes approximating the domain. This system of ODEs can then be discretized in time to obtain a full discrete problem which can be solved numerically. The stiffness of the systems pose extra requirements on the stability of the methods to be used for the time discretization. For the sake of stability, an implicit time advancement scheme must be utilized to discretize the system in time and a resulting system of simultaneous implicit equations are solved at each timestep.

The numerical algorithms implemented in STORM are described in chapter 2. Chapter 3 describes a new mechanistic based moving boundary model for PEB. Chapter 4 describes a revised model for polymer silylation. The model needed to simulate the wet development step of BLR process is described in chapter 5 and the O_2 RIE dry development model for surface imaged resist processes is described in chapter 6. Chapter 7 demonstrates simulation examples of these models and their applications to CAR, BLR and TSI. Simulation demonstration of special technology issues in 193nm lithography such as line end shortening (LES) in DUV resist and line edge roughness (LER) in surface imaged resist processes are also presented in chapter 7 before concluding this report in chapter 8.

STORM program release information can be obtained at the following web site, http://microlab.eecs.berkeley.edu/~ebo.

CHAPTER 2 Numerical Algorithms

Current applications of STORM focus on a class of nonlinear moving boundary model-equations often encountered in modeling deep submicron resist processes. These model equations take on the form of partial differential equations (PDEs). An approach suitable for solving these model-equations is to develop a *semi-discrete* analogue of the PDEs where the PDEs are discretized in space using the Finite Element Method (FEM) [14]. This consists of a discretization of a domain of interest, into elements with discrete endpoints, or nodes. The space discretization results in a system of stiff ordinary differential equations (ODEs) with the system size proportional to the number of nodes approximating the domain. This system of ODEs can then be discretized in time to obtain a full discrete problem which can be solved numerically. The stiffness of the systems pose extra requirements on the stability of the methods to be used for the time discretization. For the sake of stability, an implicit time advancement scheme must be utilized to discretize the system in time and a resulting system of simultaneous implicit equations are solved at each timestep. This chapter describes the space and time discretization algorithms used in STORM.

2.1 Finite Element Space Discretization

The STORM simulator requires the user to provide a *semi-discrete* form of the PDEs using the finite element method. To illustrate the weak formulation procedure used for the discretization process, we consider the following linear parabolic problem

$$\frac{\partial}{\partial t}U(x,t) - \nabla \bullet (D\nabla U(x,t)) = f(U(x,t)) \qquad \text{in } \Omega \times I \qquad (2.1)$$

$$U = 0 \qquad \text{on } \Gamma \times I \qquad (2.2)$$

$$U(x, 0) = U^0 \qquad (2.3)$$

The weak formulation of (1) reads as follows: Find $U(t) \in H_0^1(\Omega), t \in I$,

$$(\dot{U},V) + a(U;U,V) = (f(U),V) \qquad \forall V \in H_0^1(\Omega), t \in I \qquad (2.4)$$

such that

$$U(0) = U^0$$

where

$$(\alpha, \beta) = \int_{\Omega} \alpha\beta d\Omega \quad \text{and} \quad a(U;(W, V)) = \int_{\Omega} D\nabla W\nabla V d\Omega$$

The space $H_0^1(\Omega)$ is a Hilbert space consisting of functions V defined on Ω which together with their first derivatives are square-integrable and are zero on $\Gamma = \partial\Omega$. The reader interested in the definitions of Hilbert spaces should consult [14]. For the sake of discretization, we let Ψ_h be a finite dimensional subspace of $H_0^1(\Omega)$ with basis $\{\varphi_1, \ldots, \varphi_m\}$. Thus, we have the following semi-discrete analogue of (2.4): Find $U_h(t) \in \Psi_h, t \in I$, such that

$$(\dot{U}_h,V) + a(U_h; U_h,V) = (f(U_h),V) \qquad \forall V \in \Psi_h, t \in I \qquad (2.5a)$$

$$(U_h(x, 0), V) = (U^0, V) \qquad \forall V \in \Psi_h \qquad (2.5b)$$

Let us rewrite (3) using the representation

$$U_h(x, t) = \sum_{i=1}^{M} U_i(t)\varphi_i(x) \qquad t \in I \qquad (2.6)$$

Using (4) and taking $V = \varphi_j$, $j = 1, \ldots, M$, in (2.5), we get

$$\sum_{i=1}^{M} \dot{U}_i(t)(\varphi_i, \varphi_j) + \sum_{i=1}^{M} U_i(t)a(\varphi_i, \varphi_j) = (f, \varphi_j) \quad j = 1, \ldots, M, \quad t \in I$$

$$\sum_{i=1}^{M} U_i(0)(\varphi_i, \varphi_j) = \left(U^0, \varphi_j\right) \qquad j = 1, \ldots, M \quad (2.7)$$

or in a matrix form:

$$M \cdot \dot{U} + KU = F \qquad (2.8)$$

This can be written in the usual ODE system notation as:

$$M \cdot \dot{U} = g(U) \qquad \text{where} \qquad g(U) = F - K \cdot U \qquad (2.9)$$

$$m_{ij} = (\varphi_i, \varphi_j) = \int_{\Omega} \varphi_i \varphi_j dx$$

$$k_{ij} = a(\varphi_i, \varphi_j) = \int_{\Omega} D \nabla\varphi_i \cdot \nabla\varphi_j dx$$

$$F_i = (f(t), \varphi_i)$$

K is known as the stiffness matrix, M is the time derivative matrix or the mass matrix and F is the forcing vector or the load vector. K and M are global matrices in the sense that they contain information about the whole domain Ω. In practice, the elements k_{ij} and m_{ij} are computed by summing the contributions from the different elements discretizing the domain. STORM uses triangular elements to discretize the domain.

2.1.1 Polymer linear viscoelastic model

Resist materials are observed to behave viscoelastically below T_g and rubber-like above T_g [15]. The compaction or swelling of the polymer matrix during the relaxation of the polymer can induce mechanical stress in the resist film. If the polymer mechanical properties depend nonlinearly on the stress, the mechanics of the material is said to be non-linear. We assume a general linear viscoelastic model assuming that the polymer deviatoric strain rate depends linearly on the deviatoric stress.

We relate the mechanical properties of the polymer to the stress through the following constitutive equations [2]:

$$\dot{\varepsilon} = \dot{\varepsilon}' + \dot{\varepsilon}'' \qquad \sigma' = \sigma' + \sigma''$$

$$\dot{\varepsilon}_{xx} = \frac{\partial v_x}{\partial x} \qquad \dot{\varepsilon}_{yy} = \frac{\partial v_y}{\partial y}$$

$$\dot{\gamma}_{xy} = \frac{\partial v_x}{\partial y} + \frac{\partial v_y}{\partial x} \qquad \tau = \frac{\eta}{G}$$

$$\frac{\partial}{\partial t}\sigma' + \frac{\sigma'}{\tau} = G D\dot{\varepsilon}' \qquad D = \begin{bmatrix} 2 & 0 & 0 & 0 \\ 0 & 2 & 0 & 0 \\ 0 & 0 & 2 & 0 \\ 0 & 0 & 0 & 1 \end{bmatrix}$$

$$\sigma'' = 3K\Delta\dot{\varepsilon}'' + \sigma_0$$

v : deformation rate

$\dot{\varepsilon}'$: Shear strain rate

$\dot{\varepsilon}''$: Volumetric strain rate

σ' : Shear stress

σ'' : Hydrostatic pressure

η : Viscosity

G : Elastic shear modulus

K : Elastic bulk modulus

τ : relaxation time constant

2.1.2 Discretization of the linear momentum balance equation

To simulate polymer deformation, forces at the boundary are related to the rate of change of the dependent variables that causes volume expansion or shrinkage in the polymer during the resist process. In the case of a fast reaction, we can assume that the volume displacement in the system is only a function of the rate of change of the expanding or shrinking species at the reacted/unreacted boundary, allowing us to neglect the bulk forces in the system [3].

This approximation is valid for the model equations under consideration, since these processes exhibit a sharp reacting front which propagates inside the resist material. Under this assumption, the product of the variational of the strain rate and the stress in the system is expressed as follows [2]:

$$\int_{\Omega^t} (\delta\varepsilon^{\dot{T}} \cdot \sigma) d\Omega = \int_{\Omega^t} (\delta\mathring{\varepsilon}' + \delta\mathring{\varepsilon}'')(\sigma' + \sigma'') d\Omega$$

where the stress and strain rate vectors have been decomposed into orthogonal shear and dialational components such that the product of shear and dialational components is identically zero. The expression in terms of the velocity profile is stated as follows:

$$\delta v^T\left[\int_{\Omega^e} L'^T \eta D L' d\Omega + \int_{\Omega^e} L''^T \alpha L''\right] v = \delta v^T \int_{\Gamma^e} f d\Gamma$$

where η is the viscosity of the system and α is chosen to simulate the incompressibility of the polymer. L' and L'' are given by

$$L' = \begin{bmatrix} \left(\frac{2}{3}\right)\frac{\partial}{\partial x} & -\left(\frac{1}{3}\right)\frac{\partial}{\partial y} \\ -\left(\frac{1}{3}\right)\frac{\partial}{\partial x} & \left(\frac{2}{3}\right)\frac{\partial}{\partial y} \\ -\left(\frac{1}{3}\right)\frac{\partial}{\partial x} & -\left(\frac{1}{3}\right)\frac{\partial}{\partial y} \\ \frac{\partial}{\partial y} & \frac{\partial}{\partial x} \end{bmatrix}, L'' = \begin{bmatrix} \left(\frac{1}{3}\right)\frac{\partial}{\partial x} & \left(\frac{1}{3}\right)\frac{\partial}{\partial y} \\ \left(\frac{1}{3}\right)\frac{\partial}{\partial x} & \left(\frac{1}{3}\right)\frac{\partial}{\partial y} \\ \left(\frac{1}{3}\right)\frac{\partial}{\partial x} & \left(\frac{1}{3}\right)\frac{\partial}{\partial y} \\ 0 & 0 \end{bmatrix}$$

and v is defined by the finite element discretization interpolation functions and nodal velocity values. Since this expression must hold true for any arbitrary variation in the velocity profile we can write the following expression $[K][v] = F$, where

$$K = K' + K'' \quad K'' = \int_{\Omega^e} L''^T \alpha L'' d\Omega \quad K' = \int_{\Omega^e} L'^T \eta D L' d\Omega \quad F = \int_{\Gamma} f d\Gamma$$

K can be interpreted as the stiffness matrix relating the movement of nodes of the system through equivalent spring constants [3], which are a function of the mechanical properties of the polymer and the forces applied to it. The individual entries of K are given by

$$K_{ij} = \int_{\Omega_e} (L'\psi_i)^T \eta D(L'\psi_j) + (L''\psi_i)^T \alpha(L''\psi_j) d\Omega$$

and

$$F_i = \int_{\Gamma} \psi_i f d\Gamma$$

2.2 BDF2 Time Discretization

The BDF2 time advancement equation is of the following form:

$$\dot{U}_{j+1} = \frac{(U_{j+1} - \tilde{U})}{c(h_1, h)} \quad \text{where} \quad \tilde{U} = a(h_1, h) \cdot U_j + b(h_1, h) \cdot U_{j-1}$$

The weight values *a, b,* and *c* are given by the following expressions:

$$a(h_1, h) = 1 - b$$

$$b(h_1, h) = -\frac{h^2}{h_1^2 + 2 \cdot h_1 \cdot h}$$

$$c(h_1, h) = h + h_1 \cdot b$$

where h and h_1 are the current and previous timestep respectively. Approximating $\dot{U}$ with BDF2 time advancement scheme in equation (5), we get the discrete form.

$$M \cdot \frac{(U_{j+1} - \tilde{U})}{c} = g(U_{j+1})$$

This implicit time advancement requires Newton iterations for its solution. The following is adapted from [16].

2.2.1 Predictor for the initial Newton guess

The predictor for the initial Newton guess for the Newton solution U_{j+1} is a quadratic extrapolation from the three previous steps U_j, U_{j-1}, U_{j-2}. The divided difference form of the Lagrange extrapolation error (predictor error) $PE = U[t_{j+1}, t_j, t_{j-1}, t_{j-2}] \cdot h \cdot (h + h_1) \cdot (h + h_1 + h_2)$ is used to control the timestep, allowing accurate predictions of the system solution to ensure fast convergence of the Newton method. The predictor error requires knowledge of the converged solution which is not available. Thus, one makes the assumption that the predictor error of the current timestep is the same as the predictor error of the previous timestep. One then checks for the validity of this assumption after the converged solution is obtained and accepts or rejects the timestep based on how close the assumed predictor error is to the actual predictor error.

The time step control scheme is as follows:

1. Estimate PE_{est} using the four previous timesteps $U_j, U_{j-1}, U_{j-2}, U_{j-3}$
2. Calculate the timestep h such that PE_{est} is below some predictor error tolerance.

3. Use this h to calculate the initial Newton guess V.
4. Calculate the PE_{act} and compare with PE_{est}
5. If PE_{est} and PE_{act} are close enough, accept this timestep h. If not, half h and repeat steps (3), (4) and (5).

2.2.2 The Modified Newton method for BDF2

Newton's method involves linearizing the residual function $R(U) \equiv M \cdot (U - \tilde{U}) - c \cdot g(U) = 0$ about the latest iterate [17]. Thus, if $\bar{U}$ is the latest iterate, Newton seeks the next iterate $\bar{U} + \delta U$ from the approximation $R(\bar{U} + \delta U) \approx R(\bar{U}) + R'(\bar{U}) \cdot \delta U$ where $R' \equiv J$ is the Jacobian matrix. Instead of updating J at each iteration, J is only updated when necessary (i.e. when convergence fails with an old J) [18]. So to get the Newton correction δU one solve the linear systems $J \cdot \delta U = -R(\bar{U})$ Note that $J = M - c \cdot g'(\bar{U})$. J is a sparse matrix so an efficient sparse matrix linear solver is required to solve for δU. STORM uses SuperLU direct sparse matrix solver [19].

2.2.3 The Krylov Subspace Newton Convergence Accelerator

In order to improve the convergence characteristics, we employ Miller's Krylov subspace accelerator[17]. Beginning with the initial Newton guess y_0, the accelerator first preconditions the residual equation with the Jacobian to get

$$f(y_0) = -J^{-1} \cdot R(y_0) = r_0$$

the initial residual. Assuming that

$$f(x+z) = f(x) - A \cdot z$$

it then solves the linear residual correction equation

$$f(y_0 + v_1) \equiv r_0 - A \cdot v_1 = 0$$

to get the correction vector v_1 the next iterate $y_1 \equiv y_0 + v_1$ and $Av_1 \equiv f(y_0) - f(y_1)$. Thus at the kth step, the set of vectors $\{v_1, v_2, \ldots, v_k\}$ and $\{Av_1, Av_2, \ldots, Av_k\}$ are accumulated. The general algorithm approximates the solution of the kth residual correction equation

$$f(y_k + v) \equiv r_k - A \cdot v = 0$$

by letting w_{k+1} be the element in the subspace $V_k \equiv \mathrm{span}\{v_1, v_2, \ldots, v_k\}$ such that $\|r_k - Aw_{k+1}\|_2$ is minimized. Thus one solves the resulting linear least squares problem to obtain the desired correction w_{k+1}. The reader interested in rigorous treatment of this method should consult [17].

2.2.4 The Starting procedure

The BDF2 algorithm as described above is a multi-step method requiring four solution vectors. Thus a starting procedure is needed to generate these solution vectors

in order to proceed with the BDF2 algorithm. The Crank-Nickelson time advancement scheme is used followed by two steps of BDF2 with a fixed timestep. This gives the four solution vectors (3 + initial vector) needed to start the full BDF2 algorithm.

CHAPTER 3

Modeling Post Exposure Bake

3.1 Introduction

Chemically amplified resist (CAR) systems are characterized by a trade-off between process latitude and exposure sensitivity. Exposure latitude has been observed to decrease with increasing PEB temperature while exposure sensitivity improves at these higher temperatures [20]. This degradation of process latitude with increasing temperature is attributed to the enhancement of acid diffusion at higher temperatures. The relative impact of diffusion on smaller feature sizes has led to intensive investigation of the post exposure bake (PEB) reaction/diffusion mechanisms to gain better understanding of physical parameters affecting the relief image formation.

Several models have been proposed to describe the physical and chemical processes that occur during PEB[20][21]. Most of the physical models available in the literature differ only in the type of diffusion used to describe the acid transport mechanism. The diffusion types range from simple Fickean [21] to algebraic and exponential concentration dependent diffusion [22]. These models usually give adequate predictions of the relief image for the PEB times of interest. However, recent results of acid diffusion experiments show negligible acid diffusivity in polyhydroxysterene (PHOST), a typical polymer resin in CAR [23]. On the other hand, when the PHOST polymer is grafted with t-BOC protecting groups, the acid catalyzed reaction was observed to advance the protected/deprotected t-BOC interface. Furthermore, for long PEB times, the reactions events were observe to decrease dramatically. These observations verify the reaction driven diffusion model for PEB [24]. However, this model assumes that the diffusivity is an exponential function of the reacted group concentration (PHOST) and suggests a rapid acid diffusion in the reacted material. Since these recent experimental results show negligible acid diffusion in the reacted material, we propose a new mechanistic based moving boundary transport model based on free volume generation assumptions.

3.2 Moving Boundary model for PEB

The model takes into account the following processes during the transformation of the protected groups into deprotected groups.

1. Creation of deprotected sites and volatile groups by-products
2. Diffusion and desorption of volatile groups
3. Generation of free volume content during volatile group desorption
4. Influence of free volume content on the acid diffusion properties
5. Polymer densification during elimination of free volume content (polymer relaxation)
6. Acid loss to the ambient due to desorption of acid in the presence of free volume content
7. Acid loss to the ambient due to base contamination

The following physical model explains the above considerations. During PEB, the acid catalyzes a thermally induced reaction that deprotects the protected groups (P). Volatile by-products (V) are created during this reaction. The volatile groups have appreciable mobility in polymer. Thus, they desorp from the resist material, generating a free volume content (F) in the resist [25]. Since PEB temperatures are below the glass transition temperature (Tg) of the resist, the resist is considered to behave as a glassy polymer. Glassy polymers do not respond immediately to change in their equilibrium state [26]. Thus, the elimination of free volume after the volatile group desorption will tend to be time dependent. The rate of densification of the polymer during the elimination of the free volume content will be characterized by the relaxation time of the polymer. If this relaxation time is large compared to the characteristic diffusion time, then significant diffusion of the acid can occur before the polymer densification suppresses the diffusion and prevents the acid in the densified region from taking further part in the diffusion process. Thus, while the acid concentration remains essentially constant during PEB, only a limited number of acid molecules at the deprotected/protected interface can freely diffuse. This is because after the densification of the initially exposed region of the resist, acid molecules in this region become immobile. The free volume content needed to facilitate acid diffusion are generated only at the deprotected/protected interface where reaction is taking place. Figure (1b) illustrates this process. It is assumed that sharp boundary surface moves through the resist poly-

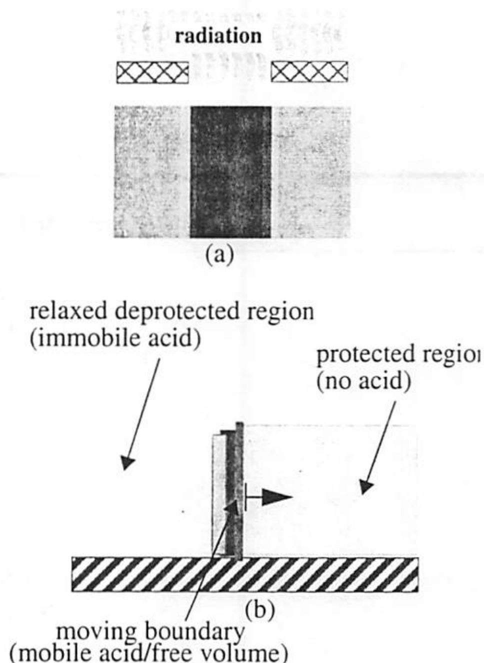

Fig. 1.(a) Acid concentration gradient after exposure.
(b) physical mechanisms governing acid transport.

mer. This boundary separates a densified region in which all acid molecules are immobile from one in which the acid concentration is zero.

The symbols used in this model is presented here for ease of reference:

H : acid group concentration

P : protected group concentration

V : volatile group state concentration

F : free volume content state concentration

A : deprotected sitesconcentration

k_r : reaction rate function

k_0 : maximum reaction rate constant

k_{des} : volatile group desorption rate constant

k_1 : parameter for acid loss due to desorption

k_2 : parameter for acid loss due to base contamination

D : acid diffusivity function

D_p : acid diffusivity in polymer

D_o : acid diffusivity in the presence of free volume content

t_r : polymer relaxation time

3.2.1 Diffusivity model

The influence of free volume content on the diffusion properties of glassy polymers is described in [27]. Since acid has negligible diffusivity in polymers in structural equilibrium, we assume that acid only diffuses in the presence of free volume content. This assumption is only valid for the case of nonvolatile acids. If the acid generated upon exposure is volatile, then the intrinsic acid diffusivity in the polymer can be appreciable even in the absence of reaction event. The reaction creates free volume contents, making the diffusion a reaction driven mechanism. These reaction events are confined at the deprotected/protected resist interface. Therefore, acid diffusion only takes place at the sharp boundary surface where the generation of free volume is taking place. This suggests a dependence of the diffusivity on the free volume concentration. A diffusion model that can be predicted theoretically using free volume arguments is the Fujitu-Doolittle equation [28]. To present a general diffusion model that is consistent with experimental results, we adapt the Fujitu-Doolittle equation to take into account the negligible acid diffusivity in the absence of free volume. We model the diffusivity function as

$$D = D_p + D_o\left(\exp\left(\frac{\omega F}{1 + \upsilon F}\right) - 1\right)$$

where D_o, D_p, ω and υ are constants.

3.2.2 Reaction Rate model

Since the reaction is driven by the acid catalyst, the reaction events can be modeled as a probability function of the catalyst concentration, where the higher the concentration, the higher the number of reaction events. Experimentally, it has been observed that at a given temperature, there is an upper limit to the amount of acid concentration which can catalyze the reaction [23]. Excess acid concentration beyond this limit has negligible effect on the number of reaction events. Thus, reaction rates above this limit is assumed to be constant. This motivates the following dependence of the reaction rate parameter on acid concentration.

$$k_r = k_0(1 - \exp(-\alpha H))$$

3.2.3 Polymer relaxation

PEB model as described above consist of two complex moving boundary problems; one in which the deprotected boundary (deprotected/protected interface) advances inside the resist material and another in which deprotected regions continuously shrink. (i.e., no conservation of volume). The characteristic time needed for the polymer matrix to reorganize itself to eliminate the free volume content is called the polymer relaxation time (t_r). We assume that the volume shrinkage rate is proportional to the free volume content concentration. We have

$$\frac{\partial}{\partial t}Vol = -\beta\frac{F}{t_r}$$

3.2.4 PEB diffusion/reaction kinetics

During the PEB step, the photo-generated acid catalyzes a thermally induced reaction of the protected group following the following chemical equations:

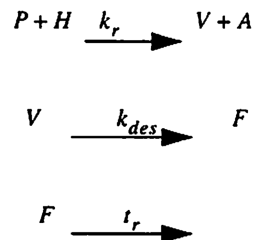

$$P + H \xrightarrow{k_r} V + A$$

$$V \xrightarrow{k_{des}} F$$

$$F \xrightarrow{t_r}$$

3.2.5 Differential Equations

The following set of coupled nonlinear partial differential equations describe the proposed PEB model:

$$\frac{\partial P}{\partial t} = -k_r PH \qquad \frac{\partial A}{\partial t} = k_r PH$$

$$\frac{\partial V}{\partial t} = k_r PH - k_{des} V \qquad k_r = k_0(1 - \exp(-\alpha H))$$

$$\frac{\partial F}{\partial t} = k_{des} V - \frac{F}{t_r} \qquad D = D_0 + D_f\left(\exp\left(\frac{\omega F}{1 + \upsilon F}\right) - 1\right)$$

$$\frac{\partial H}{\partial t} = \nabla(D \nabla H) \qquad \frac{\partial}{\partial t} Vol = -\beta \frac{F}{t_r}$$

3.2.6 Boundary conditions

The air-polymer interface can be described by assuming that the flux of the acid groups is driven by the acid concentration, free volume content concentration and base contaminants near the air-polymer interface. We model this as

$$-D\left(\frac{\partial H}{\partial n}\right)_{\text{int air-polymer}} = -k_1 HF - k_2 H$$

Assuming impermeable boundary conditions at the substrate polymer interface, we have that

$$-D\left(\frac{\partial H}{\partial n}\right)_{\text{int surface-polymer}} = 0 \qquad -D\left(\frac{\partial V}{\partial n}\right)_{\text{int surface-polymer}} = 0$$

3.3 Simplified PEB Models

The proposed model attempts to capture the physical mechanisms of the PEB process at the expense of higher complexity in the model. The number of parameters needed to apply the above model to existing resist systems is too large, making design of experiments (DOE) for parameter extraction prohibitively expensive. To make this model practical, basic assumptions have to be made to simplify the model. We make the following assumptions in order to simplify the model:

1. Desorption rate (k_{des}) of the volatile groups is much larger than the relaxation rate ($1/t_r$)
2. Intrinsic acid diffusivity in polymer (D_p) is zero (i.e. acid is nonvolatile)
3. The effects of acid loss to ambient on PEB is negligible
4. Base contamination in the ambient is negligible

Assumption (1) allows us to ignore the volatile group concentration and model the chemical reaction as:

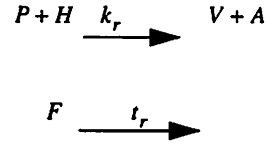

Since we have direct conversion of protected groups (P) to deprotected groups (A), we can also ignore keeping track of the protected group concentration by representing it as (P_o-A), where P_o is the initial protected group concentration. Assumptions (3) and (4) allows the boundary condition parameters to be set to zero. These assumptions lead to the following simplified set of equations which will be referred to as MBT (moving boundary transport) model in subsequent sections:

$$\frac{\partial A}{\partial t} = -k_r(P_0 - A)H \qquad D = D_0\left(\exp\left(\frac{\omega F}{1+F}\right) - 1\right)$$

$$\frac{\partial F}{\partial t} = k_r(P_0 - A)H - \frac{F}{t_r} \qquad k_r = k_0(1 - \exp(-\alpha H))$$

$$\frac{\partial H}{\partial t} = \nabla(D\nabla H) \qquad \frac{\partial}{\partial t}Vol = -\beta\frac{F}{t_r}$$

If we assume that the volatile group by-products have negligible effects on the PEB reaction/diffusion kinetics, we can arrive at an even simpler set of equations. The only drawback of this assumption is that for long enough PEB times, the model will predict that the acid will diffuse through the entire resist and deprotect the whole resist matrix. Since experimental data shows that deprotection of unexposed regions of the resist saturates for long PEB times [29], a further acid loss assumption has to be incorporated in the model to make it useful. Furthermore, a non-integer reaction order has to be introduced to better match experimental results. Under these assumptions, we will have the following chemical and differential equations to describe the PEB process, hereafter referred to as the Case II model:

$$\frac{\partial A}{\partial t} = -k_r(P_0 - A)H^m$$

$$\frac{\partial H}{\partial t} = \nabla(D\nabla H) - k_l H$$

$$D = D_0 \quad \text{or} \quad D = D_0\exp(\omega A)$$

where m is the reaction order and k_l is the acid loss rate constant. If D is chosen to be constant, then the above model is the fickean diffusion model of PEB available in the literature [21]. If D is chosen to be exponential function of the deprotected group concentration, then the above model becomes the case II type diffusion PEB model available in the literature [24]. In comparing the MBT model and the case II model, we see that the number of parameters needed to be extracted experimentally to apply the models are comparable. The MBT model requires k_o, α, t_r, D_o, w and β extracted whereas the Case II model requires k_r, k_l, D_o, m, and w extracted. The number of parameters for the MBT model can be the same as that for the Case II model if the user is only interested in predicting the extent of deprotection and latent image formation without resist shrinkage. This is often times the case and so β can usually be ignored. Thus, although the MBT model and the Case II model can have the same DOE complexity, the MBT model offers a much more accurate prediction of experimental results since it is more physical and mechanistic based than the case II model.

CHAPTER 4 Modeling Silylation

4.1 Introduction

Silylation is the process of incorporating silicon containing compound into a resist polymer. This is an important process in the top surface imaging (TSI) lithography process whereby upon exposure, the latent image is formed at the near top region of the resist. A silicon containing compound in the gas or liquid phase is diffused into the polymer and the silicon is selectively incorporated into the exposed region (negative tone) or unexposed region (positive tone) of the resist. The silicon containing region forms a SiO_2 barrier to protect the underlying resist from etching during a dry development step in an O_2 plasma.

Figure 4.1 illustrates positive tone and negative tone TSI processes. For the negative tone process, the exposure and post exposure bake activates functional groups that are capable of reacting with the silylating agent. During silylation, the silicon is selectively incorporated in the exposed region. Subsequent dry development process etches the nonexposed region away, resulting in a negative tone process. For the positive tone TSI process (Fig. 4.1b) the resist crosslinks upon exposure. During subsequent silylation, the crosslinked region inhibits the diffusion of the silylating agent, allowing selective incorporation of silicon in the nonexposed region. During the dry development process, the non silylated region is etched away, resulting in a positive image.

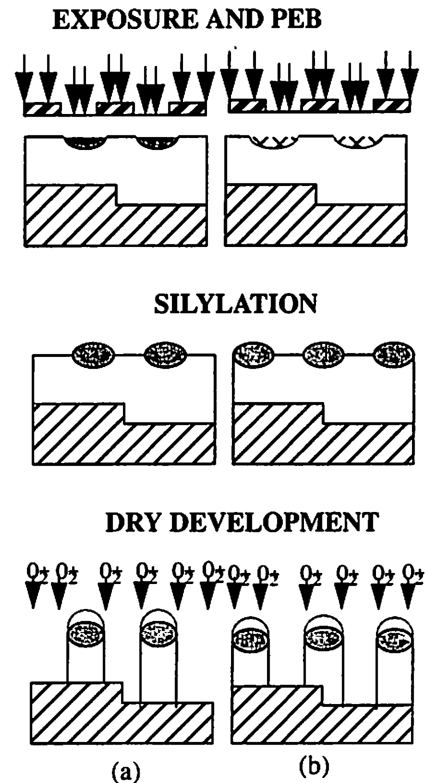

Fig. 4.1.(a) Negative tone non-diffusion enhanced TSI scheme.
(b) Positive tone diffusion enhanced TSI scheme.

Like the PEB process described in chapter 3, silylation is a moving boundary problem in which the larger molecule silylating agent continuously expands the resist polymer while a sharp silylated/unsilylated front propagates inside the resist [31]. A comprehensive model for a negative tone silylation process was first presented by Pierrat [9]. This model takes into account the reaction of the silylating agent with the hydroxyl groups of the polymer and the relaxation of the polymer after reaction. Zuniga et al proposed a two dimensional extension of the model to take into account possible stress induced reaction retardation due to polymer swelling [10]. The underlying assumptions of these models are that the silylating agent (S) reacts with the hydroxyl groups (H) to form unexpanded sites (U). The unexpanded sites then relax with some relaxation time constant t_r to form expanded sites (E). The chemical equations describing this process is as follows:

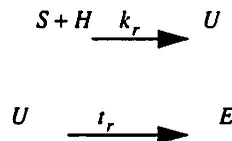

$$S + H \xrightarrow{k_r} U$$

$$U \xrightarrow{t_r} E$$

The resulting set of differential equations are [9]:

$$\frac{\partial S}{\partial t} = \frac{\partial}{\partial x} D_o exp(\omega E)\frac{\partial S}{\partial x} + \frac{\partial}{\partial y} D_o exp(\omega E)\frac{\partial S}{\partial y} - k_r SH \qquad (4.1)$$

$$\frac{\partial H}{\partial t} = -k_r SH \qquad (4.2) \qquad\qquad \frac{\partial U}{\partial t} = k_r SH - \frac{U}{t_r} \qquad (4.3)$$

$$\frac{\partial E}{\partial t} = \frac{U}{t_r} \qquad (4.4) \qquad\qquad \frac{\partial A}{\partial t} = \frac{A_f - A_i}{E_{max}} \frac{U}{t_r} \qquad (4.5)$$

$$\int_w \delta\left(\frac{\partial \varepsilon}{\partial t}\right) \sigma = \int_\Gamma \delta(v)\, f + \int_w \delta(v)\, b \quad (4.6) \qquad k_r = Aexp\left[-\frac{(Ea_1 - B\sigma)}{KT}\right] \quad (4.7)$$

where D_o is the silicon intrinsic diffusivity in the unsilylated film, k_l is the reaction rate, t_r is the polymer relaxation time, w is the reaction-diffusion coupling coefficient, and B is the stress-reaction coupling coefficient. Resist swelling, as modeled by equation (4.5), is supposed to give rise to stress and strain fields as a function of the local deformation, as calculated by equation (4.6). As illustrated in equation (4.7), such stress fields are supposed to lead to a local reduction in the reaction rate by linearly changing the activation energy of the process. The silylated/unsilylated boundary propagation is modeled by the nonlinear diffusive transport as shown in (4.1). This local enhancement with the diffusivity is a result of both the polymer expansion and the lowering of the glass transition temperature (Tg) at the reacted sites.

Though the above model is mechanistically appealing, the sequence of reaction events has to be modified since the hydroxyl group sites of the resist polymer must first expand to adsorb the larger molecule silylating agent during the reaction.

4.2 Moving Boundary Model for Silylation

We propose a general moving boundary model for positive and negative tone silylation process capable of simulating both diffusion enhanced on non-diffusion enhanced silylating schemes. This model takes into account the following:

1. Diffusion of the silylating agent in non-crosslinked region
2. Adsorption of the silylating agent at functional group sites
3. Polymer expansion during adsorption of silylating agent (polymer relaxation)
4. Reaction of the functional groups with the adsorbed silylating agent
5. Enhancement of local diffusivity at the reacted sites

An intuitive picture of the mechanisms that motivated the above considerations can be obtained as follows. During silylation, the silylating agent diffuses in the non-crosslinked region of the polymer (diffusion enhanced silylation) or the diffuses through the entire polymer (non-diffusion enhanced silylation). Since the silylating agent molecules are larger than the functional group sites, the silylating agent must be adsorbed at the functional group sites before reaction can take place. This adsorption process can be visualized by assuming that the larger silylating agent molecule must penetrate into the smaller functional group sites in order to make itself available for reaction. As a first pass, we will model the adsorbtion process by the absorbing probability equation where it is assumed that the probability that a silylating agent will be adsorbed is proportional to the silylating agent flux. During the adsorption, the polymer is displaced by the larger silicon molecule, causing it to swell at the site. We assume that the polymer adsorption/swelling rate is proportional to the polymer relaxation time (t_r). After adsorption, the silylating agent reacts with the functional groups to form the reacted sites. Since the silylated resist has lower glass transition temperature (T_g) [9], the diffusivity of the silylating agent at the reacted sites is much larger than that of the unsilylated sites. This mechanism creates a sharp moving boundary between silylated and unsilylated resist.

4.2.1 Adsorption rate model

From the above consideration, we can write the following model for the adsorption rate probability:

$$k_{ads} = \left(1 - \exp\left(-\alpha\frac{S}{t_r}\right)\right)$$

In words, the probability that a silylating agent will be adsorbed at a functional group site is proportional to the silylating agent concentration and inversely proportional to the polymer relaxation time. The higher the silylating agent concentration or the lower the relaxation time, the higher the probability of an adsorption event. Thus, the reaction rate will be proportional to the silylating agent concentration, the functional group concentration and the probability that the silylating agent will be adsorbed at the functional group sites.

4.2.2 Diffusivity model

As explained above, the local diffusivity is enhanced at the reacted sites due to the lower T_g of the polymer at these sites [9]. Since there are several silylation processes [32][8][29], a general model should account for all these processes. The Fojita-Doolittle equation for diffusion is more appealing for reacted sites enhanced diffusion since it is theoretically derived from free volume and glass transition temperature arguments [28]. To present a general diffusion model, we adapt the Fujita-Doolittle equation to take into account cross-linked regions that impedes the diffusion of the silylating agent.

$$D = D_0\exp\left(\frac{\omega R}{1 + \upsilon R} - \gamma C\right)$$

D_o is the intrinsic diffusivity of silylating agent in the resist polymer, R is the reacted sites concentration and C is the cross-linked sites concentration.

4.2.3 Polymer relaxation

As discussed above, the silylation process consists of two complex moving boundary problems; one in which the silylated/unsilylated boundary advances inside the resist material and another in which resist continuously swell during the process of silylating agent adsorption (i.e., no conservation of volume). We assume that the volume expansion rate is proportional to the change in the reacted sites concentration. This assumption yields:

$$\frac{\partial}{\partial t}Vol = \beta\frac{\partial R}{\partial t}$$

β is a parameter proportional to the size of the silylating agents molecules being adsorbed in the resist.

4.2.4 Silylation diffusion/reaction kinetics

The following chemical equations summarizes the reaction kinetics described above:

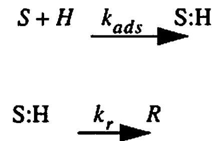

where S:H is an adsorbed site available for reaction.

4.2.5 Differential Equations

The following set of coupled nonlinear partial differential equations describe the proposed silylation model:

$$\frac{\partial S}{\partial t} = -k_{ads}k_r SH + \nabla(D\nabla S)$$

$$\frac{\partial H}{\partial t} = -k_{ads}k_r SH$$

$$\frac{\partial R}{\partial t} = k_{ads}k_r SH$$

$$\frac{\partial}{\partial t}Vol = \beta k_{ads}k_r SH$$

$$D = D_0\exp\left(\frac{\omega R}{1+R} - \gamma C\right)$$

$$k_{ads} = \left(1 - \exp\left(-\alpha\frac{S}{t_r}\right)\right)$$

$$k_r = A\exp\left[-\frac{(Ea_1 - B\sigma)}{KT}\right]$$

4.2.6 Boundary conditions

The gas-polymer interface can be described by assuming that the flux of the silylating agent is driven by the gas pressure in the reactor and by the concentration of the silylating agent in the polymer near the gas-polymer interface [9]. We model this as

$$-D\left(\frac{\partial S}{\partial n}\right)_{\text{int air-polymer}} = k_1 P_a - k_2 S$$

Assuming impermeable boundary conditions at the substrate polymer interface, we have that

$$-D\left(\frac{\partial S}{\partial n}\right)_{\text{int substrate-polymer}} = 0$$

CHAPTER 5

Modeling Wet Development

5.1 Introduction

The bilayer (BLR) process requires a wet development step to define the silicon containing resist region for subsequent O_2 reactive ion etching (RIE) dry development. Thus, a wet development model is needed to simulate BLR. STORM is a useful general framework for the many potential phenomena in wet development. Considerable amount of work has been done in modeling wet development [4][7][35][36].

The nonlinear response of the activated (deprotected or non-inhibited) sites concentration to an aqueous developer during the wet development process suggests a mechanism governed by a nonlinear moving boundary model-equation. We explore a simple resist contrast based moving boundary model that takes into account the following mechanisms:

1. Diffusion of the developer from the bulk solution to the surface of the resist
2. Adsorption of the developer at the resist surface
3. Reaction of the resist polymer with the adsorbed developer
4. Desorption of the reacted product back into the bulk of the developer
5. Enhancement of local diffusivity at developed sites

An intuitive picture of the mechanisms that motivated the above considerations can be obtained as follows. During wet development, the developer must be adsorbed by the resist surface to react with the polymer. The increase in solubility rate at the activated sites of the resist is attributed to the increase in adsorption rate at the activated sites. We will model the adsorbtion process by the absorbing probability equation where it is assumed that the probability that the developer will be adsorbed is proportional to the local activated sites concentration. This adsorption probability will be assumed to follow resist contrast curves. After adsorption, the developer reacts with the polymer to

form developed sites. These sights represent the absence of the resist polymer. The developer is then transported to the undeveloped resist surface to be absorbed. This rapid transport through the developed sites can be modeled as an enhancement in the diffusivity at the developed sites. This mechanism creates a sharp moving boundary at the surface of the undeveloped resist matrix.

5.2 Adsorption rate model

From the above consideration, we write the following model for the adsorption rate probability:

$$k_{ads} = max((1 - \exp(-\alpha(A - A_o))), k_1)$$

where A is the activated sites concentration, A_o is the threshold activated site concentration, k_1 is the adsorption probability of an unexposed resist and α is a fitting parameter. In words, the probability that a developer molecule will be adsorbed at a resist surface is proportional to the activated sites concentration. If the activated sites concentration is below a certain threshold (A_o), then the adsorption probability takes the value of that of an unexposed resist (very small positive number). The higher the activated sites concentration, the higher the probability of an adsorption event which results in higher solubility rates. This model resembles resist contrast curves as shown in figure 5.1. Figure 5.1a shows the normalized resist thickness remaining after development vs. exposure energy (after post exposure bake) [30]. Figure 5.1b shows the developer adsorption probability vs. activated sites concentration. It is assumed that there exists an activated sites concentration A_f for which the adsorption probability is 1 for all activated sites concentration more than A_f. The resist contrast γ is a measure of the steepness of the curve (a) in transition from E_o to E_f and is commonly defined as

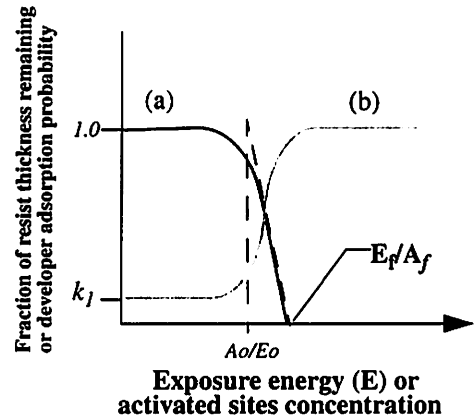

Fig. 5.1. (a) Normalized resist thickness remaining after development vs. exposure energy (after post exposure bake)
(b) Developer adsorption probability vs. activated sites concentration after post exposure bake

$$\gamma = \frac{1}{\log_{10}\left(\frac{E_f}{E_o}\right)}$$

E_o is the threshold exposure energy for dissolution. Likewise, α is a measure of the steepness of curve (b) from A_o to A_f and is assumed to be proportional to γ. Thus, α can be extracted from resist contrast curves such as in figure 5.1a. From the above considerations, the development rate will be proportional to the resist resin concentration (R), the developer concentration (Q) and the probability that the developer will be adsorbed at the resist surface.

5.3 Diffusivity model

As explained above, the local diffusivity is enhanced at the developed resist sites due to the absence of resist polymer at these sites. We assume an exponential dependence of the diffusivity on the developed sites concentration.

$$D = D_0 \exp\left(\frac{\omega P}{1 + \upsilon P}\right)$$

D_o is the intrinsic diffusivity of developer in the resist polymer and P is the developed sites concentration.

5.4 Wet development diffusion/reaction kinetics

The following chemical equations summarizes the reaction kinetics described above:

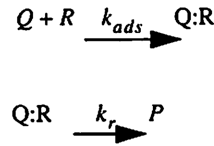

where R is the resin concentration, Q is the developer concentration Q:R is the adsorbed site available for reaction, P is the product of the reaction and k_r is the reaction rate constant.

5.5 Differential Equations

The following set of coupled nonlinear partial differential equations describe the proposed wet development model:

$$\frac{\partial Q}{\partial t} = -k_{ads} k_r Q R + \nabla(D \nabla Q)$$

$$\frac{\partial R}{\partial t} = -k_{ads} k_r Q R$$

$$\frac{\partial P}{\partial t} = k_{ads} k_r Q R$$

$$D = D_0 \exp\left(\frac{\omega P}{1 + \upsilon P}\right)$$

$$k_{ads} = max((1 - \exp(-\alpha(A - A_o))), k_1)$$

5.6 Boundary conditions

The initial resist-developer interface can be described by assuming that the flux of the developer solvent is driven by the difference in the developer concentrations at the bulk and the resist surface as well as the surface inhibition content concentration at the resist surface. We model this as

$$-D\left(\frac{\partial Q}{\partial n}\right)_{\text{int developer-polymer}} = k_1(Q - Q_s) - k_2 I$$

where I is the inhibitor content concentration. Assuming impermeable boundary conditions at the substrate polymer interface, we have that

$$-D\left(\frac{\partial Q}{\partial n}\right)_{\text{int substrate-polymer}} = 0$$

CHAPTER 6 Modeling O_2 Reactive Ion Etching for Surface Imaged Resists

6.1 Introduction

Surface imaged resist processes require O_2 reactive ion etching (RIE) dry development step to transfer the resist image defined at the near top region to the rest of the resist. In the top surface imaging (TSI) and the bilayer resist (BLR) processes, the near top region of the resist to be etched contains silicon, which converts to silicon dioxide etch mask during the dry development step. The modeling of this O_2 RIE process is necessary for the simulation of surface imaged resist processes. The difference between etching surface imaged resist processes and conventional RIE processes is that the etch mask is not prescribed before the etching process. It must be created during the etching process proper. Thus, modeling of the O_2 RIE process necessitate the modeling of SiO_2 etch mask formation during the etching.

Fig. 6.1 illustrates the dry etching process for surface imaged resists. The feed gas is assumed to be SO_2. The oxygen atoms react with the silicon to form a SiO_2 barrier. The presence of sulfur results in inhibition of reaction on the resist surface and protects the sidewalls. The resist surface is bombarded with energetic ions and surface that is not protected by barrier gets etched away. The incident energetic ions remove the sulfur, increasing the etch rate of bombarded surfaces.

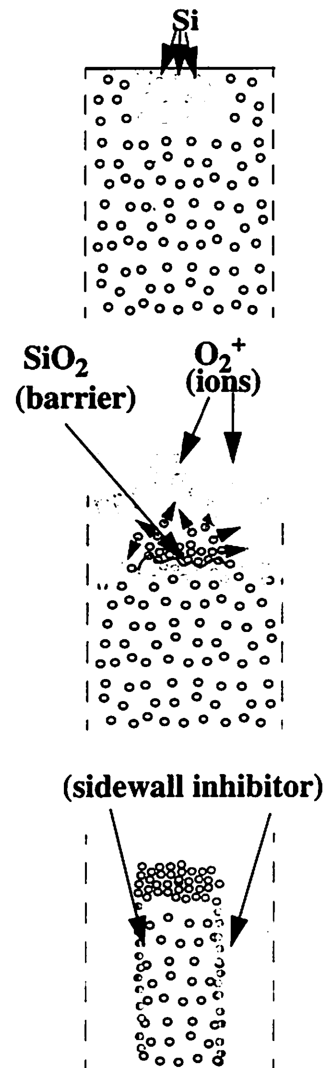

Fig. 6.1.
Schematic is dry etch process for surfaced imaged resist processes

A considerable number of plasma processing models and simulators have been developed [5][37][11][12][39][40][38]. The available simulation models attempt to capture the material removal by emulating the time evolution of the topography during the etching process. The most popular algorithm used for topographic profile simulation is the *string algorithm*, well known from the simulation program SAMPLE [5]. In this algorithm, the wafer surface is represented by a string of points connected by line segments (2D) or surface elements (3D). Depending on the implementation, the lines are moved according to the local etch rate [12].

A second algorithm for dry etch simulation is the *cell-removal method* proposed by Pelka [12]. In this approach, the complete volume of the material to be etched is described by dividing it into a matrix of little cells. These cells are removed according to the local etch conditions. Both approaches described above simulate the time evolution of the topography in order to be able to visualize the final topography after etching.

An alternative approach used in STORM is to represent the simulation domain with a grid of nodes and elements using the finite element method. The material to be etched is given some initial concentration and the time evolution of the remaining material topography is predicted by the reaction/diffusion/ion-bombardment kinetics on a fixed grid. The etched profile can then be visualized with a plotter such as MATLAB, by plotting the concentration of the remaining material. By using interpolation schemes to refining the grid, the plotter displays a sharp contrast between etched and non-etched material and leads to a more realistic profile after simulation. In this way, visualization of the final profile is left as a task of a plotter and not the grid. Most importantly, line edge roughness as observed in etched profiles of surface imaged resists can be simulated more efficiently with this approach.

6.2 O_2 RIE plasma etching model for surfaced imaged resists

We demonstrate the new approach by modeling the O_2 RIE dry development process of surface imaged resists, although the approach is applicable to all plasma etching processes. We consider the following mechanisms during the O_2 RIE dry development step:

1. Transport of oxygen (*O*) from the bulk plasma to resist (*C*) surface
2. Reaction of silicon (*S*) and *O* to form SiO_x etch barrier (*B*)
3. Adsorption of *O* by *C* surface to form *C:O* adsorbed products
4. Reaction and thermal desorption of *C:O* to form volatile products (*P*)
5. Ion enhanced desorption of *C:O* products
6. Physical sputtering of *S*
7. Physical sputtering of *B*
8. Enhancement of local diffusivity of oxygen at etched sites

The following describes the above mechanism. During the dry development step, *O* atoms (activated neutrals) diffuse to the resist surface to react with the carbon (*C*) and silicon (*S*) while energetic ions (*I*) bombard the exposed surface. The reaction of the *O* with *S* result in a SiO_x etch barrier (*B*). The adsorption *O* by *C* surface and subsequent reaction results in isotropic etching (ashing) of the resist. The ion enhances the etching rate at the surface by increasing the desorption rate of the etched products. The rate-limiting step is assumed to be desorption of *CO* gas [33]. Energetic ions can also sputter the silicon before it forms a barrier or can sputter the barrier. The absence of resist material after etching means the fresh *O* atoms can be quickly transported to the new exposed surface. We consider this as an enhancement of the local diffusivity at the etched sites.

The chemistry and physics of a plasma process is very complex, making the evaluation of all possible surface processes computationally expensive. Additional chemistry and physics can be incorporated into the above etch model, including the consideration of SO_2 feed gas (instead of O_2 feed gas) to allow for sidewall passivation by the sulfur products, physical sputtering of carbon, formation and desorption of CO_2 as an etch product, etc. These processes can be added to the above model with ease but at the cost of increased computation resources and time.

6.3 Monte-Carlo method for Ion bombardment

We assume that the energy and angle of incident of the ions arriving at the resist surface have a normal distribution about some mean value with standard deviation σ. For the energy, the mean is chosen to be proportional to the substrate bias. The mean incidence angle is chosen to be zero (normal to the surface) with $\sigma \approx 2°$ [12]. In order to distinguish different angles of incidence and different energies, Monte-Carlo methods are used. A random number generator determines the energy and angle of a incident ion. The effects of the ion on etching are then incorporated into the calculation of the state of the resist surface.

6.4 Dry development diffusion/reaction kinetics

The following chemical equations summarizes the reaction kinetics described above:

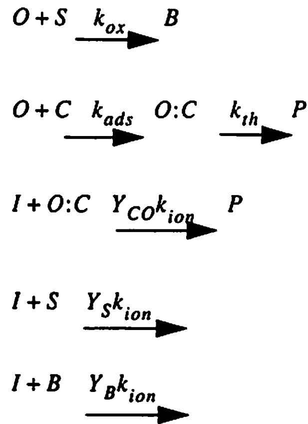

where k_{ox} is the oxidation rate constant, k_{ads} is the adsorption rate constant, k_{ther} is the thermal desorption rate constant, Y_{CO}, Y_S and Y_B are the yield of CO, S and B molecules desorped or sputtered per ion incident, and k_{ion} is proportional to the ion bombardment energy.

6.5 Diffusivity model

We assume that the plasma is generated at a high enough pressure such that the transport of the activated neutrals is governed by diffusion. As explained above, the local diffusivity is enhanced at the etched sites due to the absence of resist polymer at these sites (free space). We assume an exponential dependence of the diffusivity on the etched sites concentration.

$$D = D_0 \exp\left(\frac{\omega P}{1 + \upsilon P}\right)$$

D_o is the intrinsic diffusivity of neutrals in the resist polymer and P is the reacted product (free space) concentration.

6.6 Differential Equations

We assume that all O atoms incident on the surface react immediately to form $C{:}O$. i.e. Adsorption probability k_{ads}=1. We further assume that the desorption rate is much larger than the adsorption rate so that we need not keep track of $O{:}C$ concen-

tration. The following set of coupled nonlinear partial differential equations describe the proposed dry development model:

$$\frac{\partial O}{\partial t} = -k_{ox}OS - k_{th}OC + \nabla(D\nabla O)$$

$$\frac{\partial S}{\partial t} = -k_{ox}OS - Y_S k_{ion} IS$$

$$\frac{\partial B}{\partial t} = k_{ox}OS - Y_B k_{ion} IB$$

$$\frac{\partial C}{\partial t} = -k_{th}OC - Y_{OC} k_{ion} IOC$$

$$\frac{\partial P}{\partial t} = k_{th}OC + Y_{OC} k_{ion} IOC$$

$$D = D_0 \exp\left(\frac{\omega P}{1 + \upsilon P}\right)$$

6.7 Boundary conditions

The gas-polymer interface can be described by assuming that the flux of the oxygen atoms is driven by the gas pressure in the reactor and by the concentration of the oxygen in the polymer near the gas-polymer interface. The adsorption is assumed to be small at the barrier sites. We model this as

$$-D\left(\frac{\partial O}{\partial n}\right)_{\text{int air-polymer}} = k_1 \exp(-\alpha B) P_a - k_2 O$$

Assuming impermeable boundary conditions at the substrate polymer interface, we have that

$$-D\left(\frac{\partial O}{\partial n}\right)_{\text{int substrate-polymer}} = 0$$

CHAPTER 7 Applications of STORM

The first pass models proposed in chapters 3, 4, 5 and 6 are used as test vehicles for STORM to simulate post exposure bake (PEB), silylation, wet development and dry development. We use SPLAT and BLEACH [5] for the resist exposure simulation. Simulation results for 193nm resist applications including bilayer resist (BLR), top surface imaging (TSI) and chemically amplified resist (CAR) processes are presented in this chapter. Simulation capability of special technology issues such as line end shortening (LES) effects in DUV resist and line edge roughness (LER) in surface imaged resist processes are also presented.

7.1 Post exposure bake simulation

The results that we present in this section simulates the full model in one dimension and the simplified versions of the model, namely MBT model and Case II model in two dimension.

7.1.1 1D full model simulation results

Figure 1 gives the profiles of acid groups, protected groups, volatile groups, free volume content, and deprotected sites versus the distance into the initially protected t-BOC for the following conditions: $D_f = 1\times10^{-4}\frac{\mu m^2}{s}$, $D_v = 1\times10^{-2}\frac{\mu m^2}{s}$, $k_o = 2.0\frac{\mu m}{s}$, $k_{des} = 10.0\frac{1}{s}$, $t_r = \frac{1}{2}s$, $\alpha = 10.0$, $\omega = 5.0$, and $\nu = 1.0$. The PEB time is 60s and the simulation performance is under 30 seconds for this 1-D case on a 600MHz machine. The time arrows in these figures illustrate the time evolution of the species. The acid concentration profile shows acid diffusion only at the front where free volume content is being generated. The acid behind the front is immobile and maintains the initial profile for all times. The protected groups concentration profiles and the deprotected sites concentration exhibit a very sharp moving boundary between deprotected and protected regions. The volatile groups and the free volume content exhibits traveling waves of

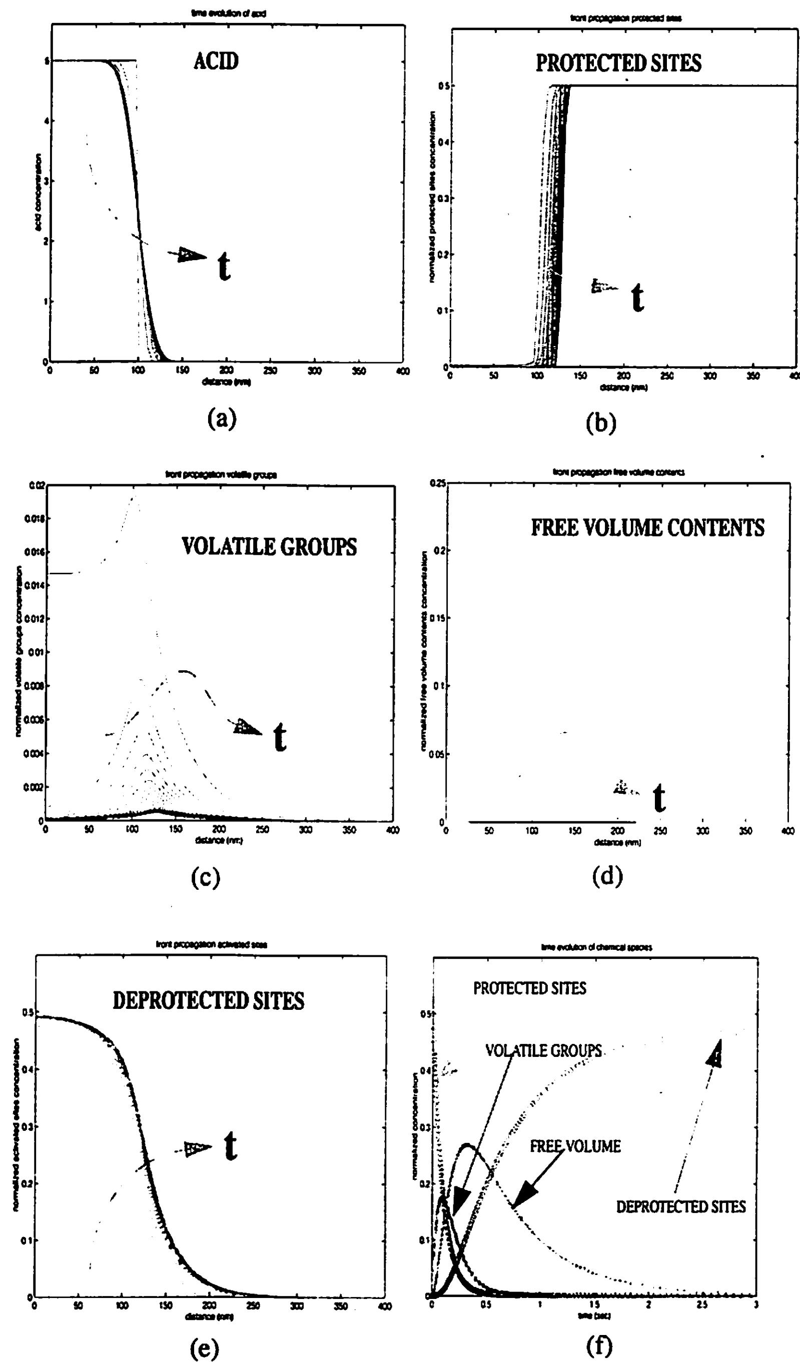

Figure 1. Front propagation of species. (a) Acid sites concentration. (b) Protected sites concentration. (c) Volatile group concentration. (d) Free volume concentration. (e) Deprotected sites concentration. (f) Time evolution of species at a fixed node.

changing profiles that rise and decay with time. The time evolution of the species at a fixed site (Fig. 2f) illustrates this phenomena.

7.1.2 2D MBT model (simplified) simulation results

Figure 2 shows the simulation results of surface imaged resist. The left hand figure shows the acid concentration in resist after SPLAT and BLEACH simulations. The figure on the right shows the deprotected sites concentration and the resist volume shrinkage. The simulation performance is under 3 minutes on the same machine.

Surface Image resist shrinkage after PEB

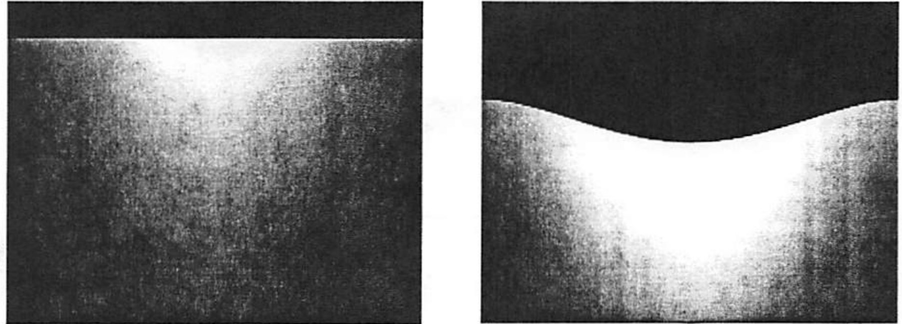

Figure 2. The left hand figure shows the acid concentration in resist after SPLAT and BLEACH simulations. The figure on the right shows the deprotected sites concentration and the resist volume shrinkage.

Figure 3 shows the PEB simulation for DUV chemically amplified resist for the case of volume shrinkage (right) and no volume shrinkage (left). Figure 3a shows the initial acid concentration. Figure 3b shows the acid concentration after 60 seconds PEB time and figure 3c shows the deprotected sites concentration after PEB_2 The following simulation parameters were used to obtain this result: $D_o = 1\times10^{-6}\frac{\mu m^2}{s}$, $P_o = 0.5$, $k_o = 1.0\frac{\mu m^2}{s}$, $\beta = 0.001$, $t_r = 3.0s$, $\alpha = 1.0$, $\omega = 100$, and $\nu = 1.0$. The simulation performance is under 10 minutes. The deprotected sights concentration exhibit a very sharp concentration gradient as predicted by the MBT model.

7.1.3 2D Case II diffusion model simulation results

Figure 4 shows PEB simulation using the Case II model. Comparing the concentration gradient of the deprotected sites at the reacted front, it can be seen that the MBT model exhibit much sharper front than the Case II model.

7.2 Silylation simulation

Fig. 5 and 6 shows the simulation results for positive and negative tone silylation schemes, respectively. The left figure of fig. 5 shows the exposure simulation results and is supposed to represent the extent of crosslinking in the film after exposure. The simulation is run for the isolated space, isolated line and dense lines (only one line is shown for dense line) cases. In fig. 6, the top figure shows the exposure (left) and post exposure bake (middle) simulation results and is supposed to represent the concentration of func-

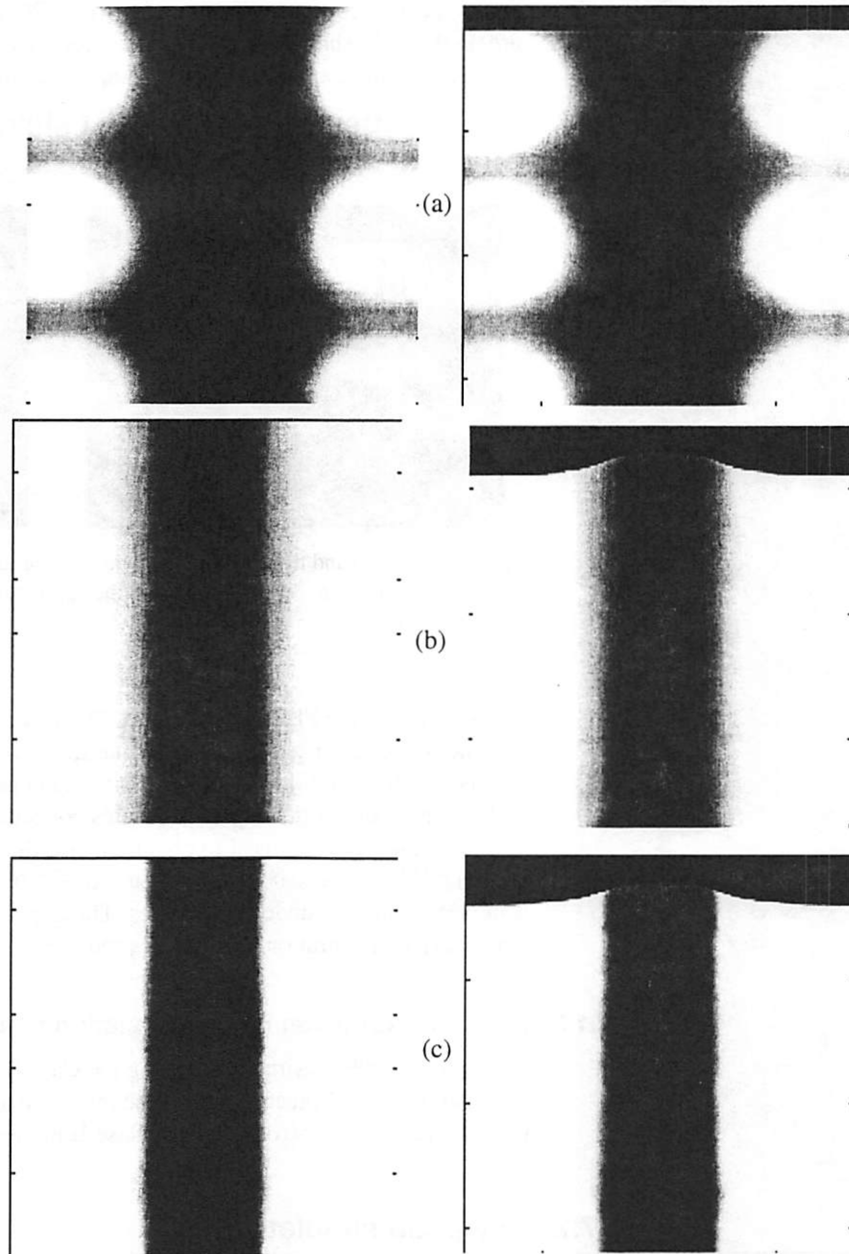

Figure 3. (a) initial acid concentration. (b) acid concentration after 60 seconds PEB time (c) deprotected sites concentration. Note the sharp contrast between protected and deprotected regions.

tional group capable of reacting with silylating agent to produce the 0.15um silylated profile shown (right).

Case II model Simulation of CAR

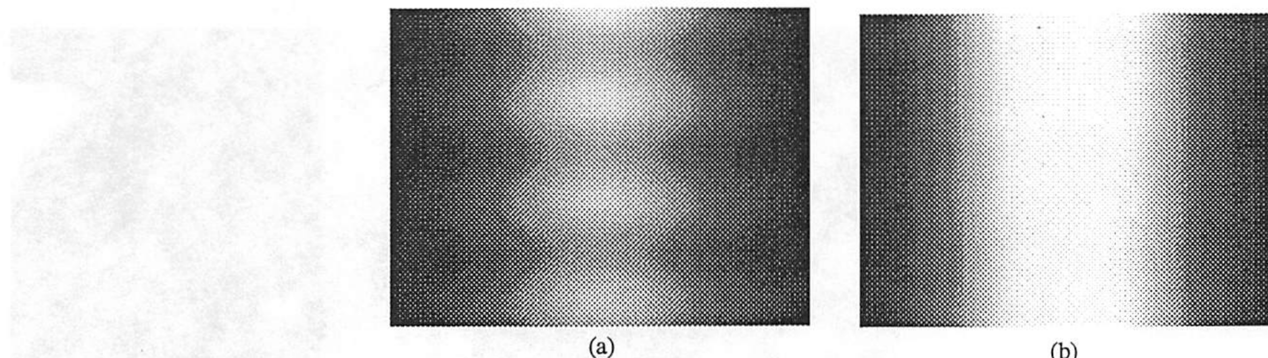

Figure 4. a) initial acid concentration. (b) deprotected sites concentration.

7.2.1 Positive tone non-diffusion enhanced silylation scheme

Isolated space

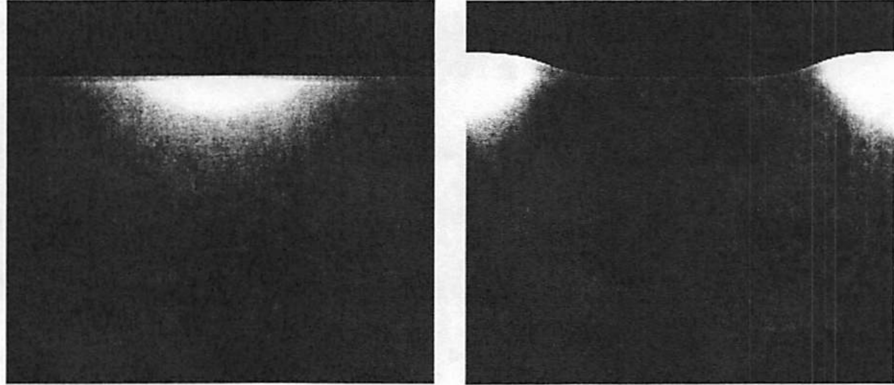

Isolated line

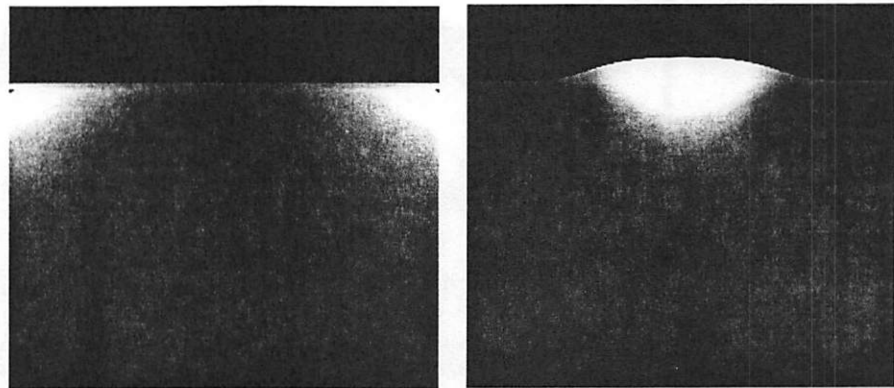

Dense lines

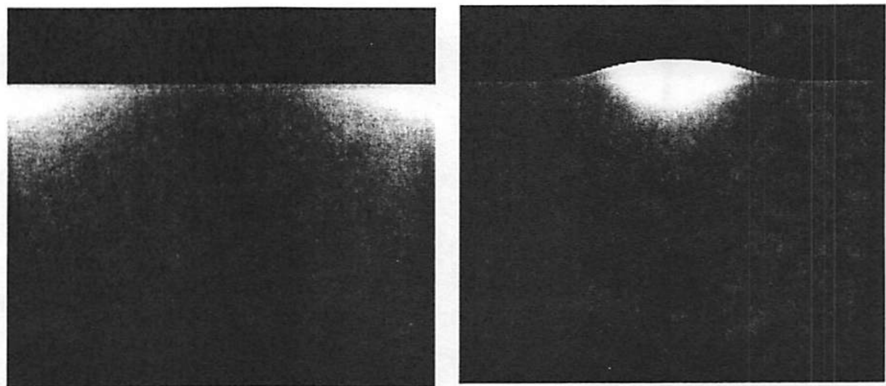

Figure 5. Simulation results for positive tone silylation scheme. The left figure shows the exposure simulation results and is supposed to represent the extent of crosslinking in the film after exposure. The simulation is run for the isolated space, isolated line and dense lines (only one line is shown for dense line) cases.

7.2.2 Negative tone non-diffusion enhanced silylation scheme

Negative tone silylation

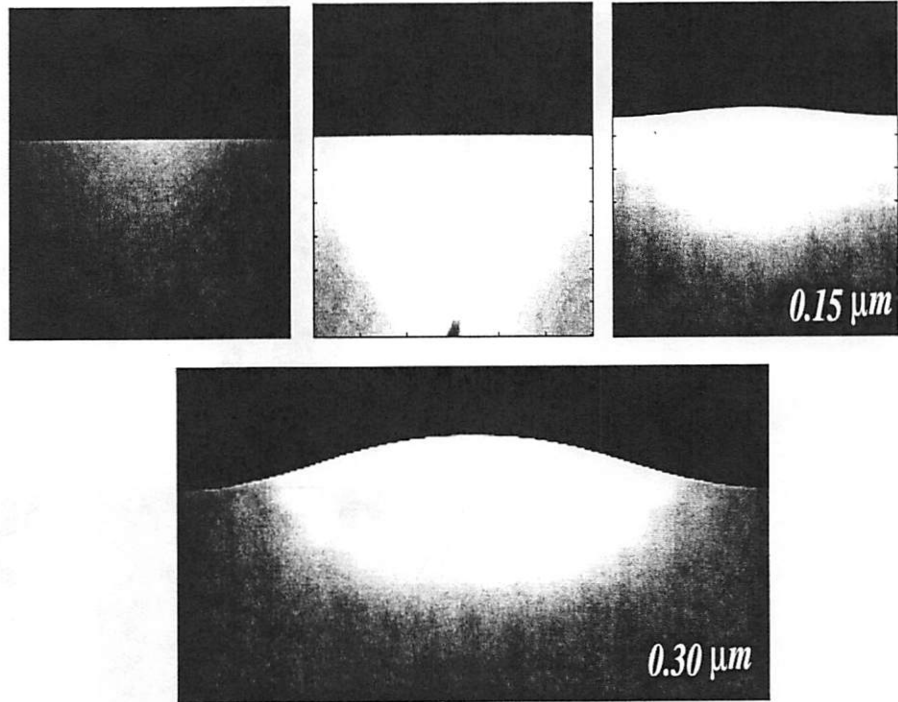

Figure6.
Simulation results for negative tone silylation scheme. Top figure shows the exposure and post exposure bake simulation results and is supposed to represent the concentration of functional group capable of reacting with silylating agent.

7.3 Wet development simulation

The simulation results for the wet development process is shown in figure 7. Fig. 7a shows the initial deprotected sites concentration. Fig. 7b shows the developer concentration at some intermediate time and the Fig. 7c shows the resist remaining at this time. Fig. 7d shows the final resist line after development. This result shows a very vertical line because a high value of α was used to represent a resist with very high contrast.

This is a good demonstration of the efficiency of STORM at simulating very nonlinear processes. The performance time is around 12 minutes.

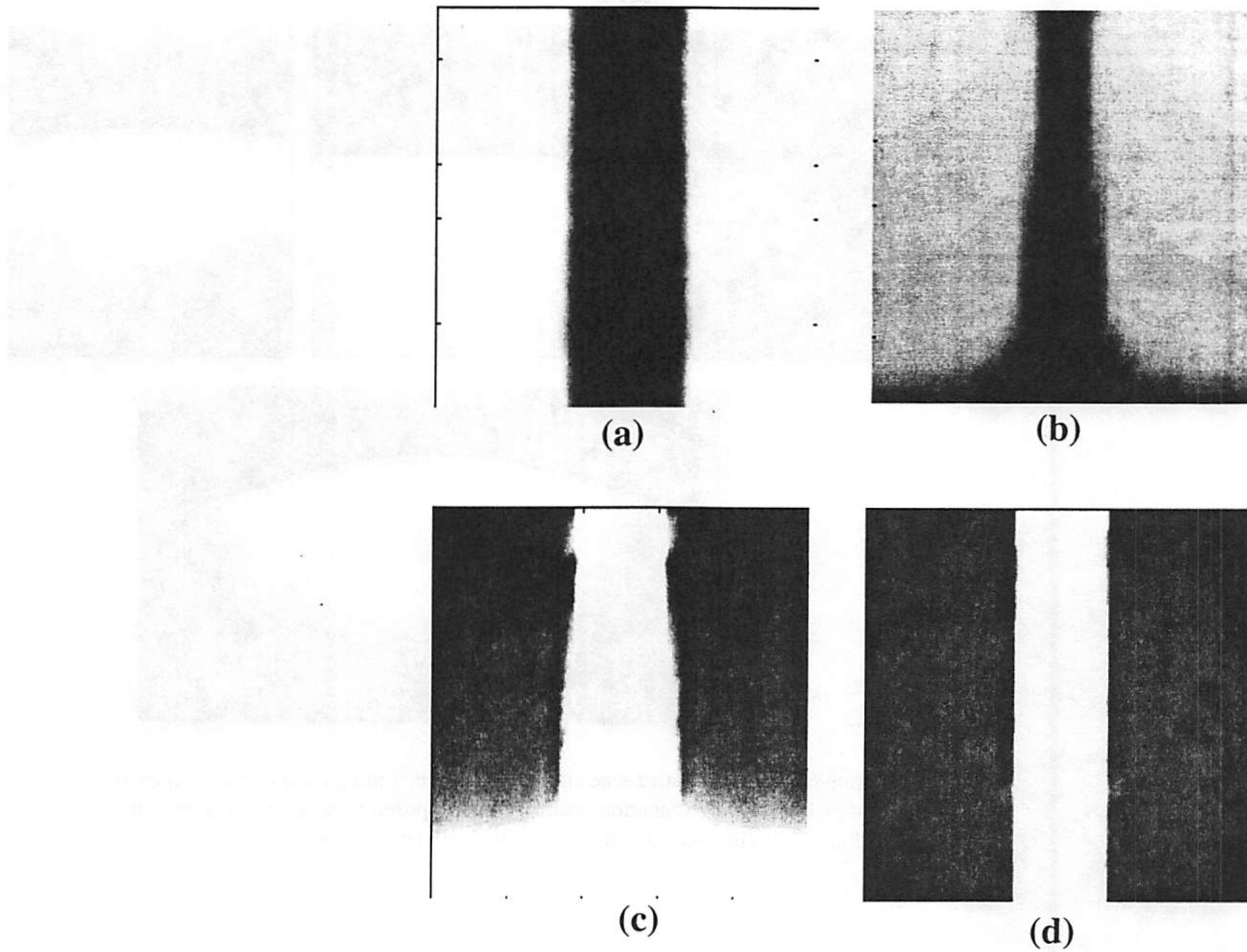

Figure 7. a) deprotected sites concentration. (b) developer concentration after some intermediate time (c) resist remaining after this time. (d) final resist line.

7.4 Dry development simulation

The dry development model simulation is by far the most challenging model for STORM. The complexity stem primarily from the nondeterministic Monte Carlo process of ion bombardment. The BDF2 algorithm described in Chapter 2 assumes that the PDE simulates a deterministic process and uses an extrapolation scheme based on previous history to predict the initial guess for the Newton iterations. Unfortunately due to the randomness of the ion bombardment, the BDF2 algorithm fails to make accurate predictions and therefore carefully take very small timestep to reduce numerical errors. Therefore for the dry development process we have to turn off the adaptive timestep control feature and use fixed timesteps to prevent BDF2 from taking very small timesteps and therefore increasing the simulation time. Because of this performance

degradation, simulation times for the dry development processes takes about 50 minutes to complete.

7.4.1 2D simulation results

Fig. 8 shows simulation results of the dry etching process for surface imaged resist. Fig.

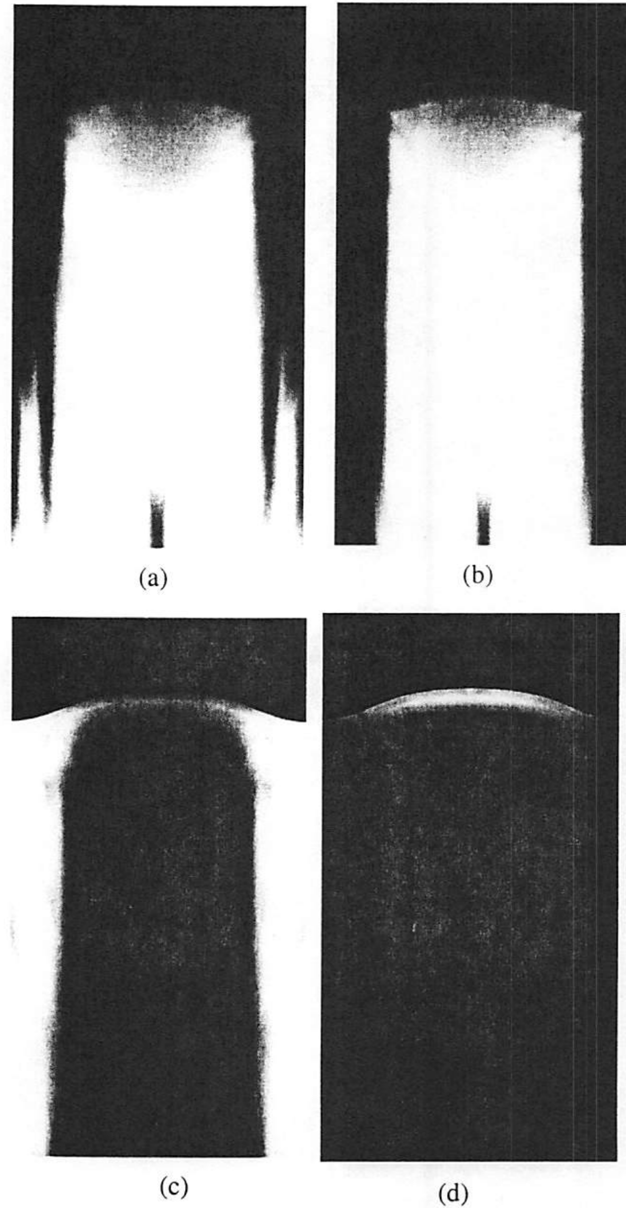

Figure 8. (a) etched profile after some intermediate time (b) final etch profile after dry development. (c) oxygen atom concentration after dry development. (d) SiOx barrier concentration.

8a shows resist remaining after some intermediate time and Fig. 8b shows the resist line after the dry etching step. Fig. 8c shows the oxygen atoms concentration and the resulting SiO_x barrier concentration protecting the unetched resist surface. The reader is advised to ignore the darker region at the bottom center of the profile. This is due to plotting error.

7.5 193nm lithography applications

We combine the above simulation results to demonstrate the capability of using STORM to aid in understanding 193nm lithography technology issues. We present simulation examples for TSI, BLR and CAR process for 193nm lithography. We also present results for LER and LES.

7.5.1 193nm Chemically amplified resists

Fig. 9 demonstrates how STORM can be used to study the extension of CAR to 193nm lithography. For the sake of simulation, we simply assume that such a CAR exists and expose the resist with 193nm light to simulate small features. Fig. 9a shows the acid concentration exhibiting standing wave effects after resist exposure. Fig. 9b shows the washing out of the standing waves in the acid profile after PEB. Fig. 9c shows the result-

ing deprotected group concentration and Fig. 9d shows the final line after wet development. Note that the resist volume shrinkage after PEB is also simulated in these figures.

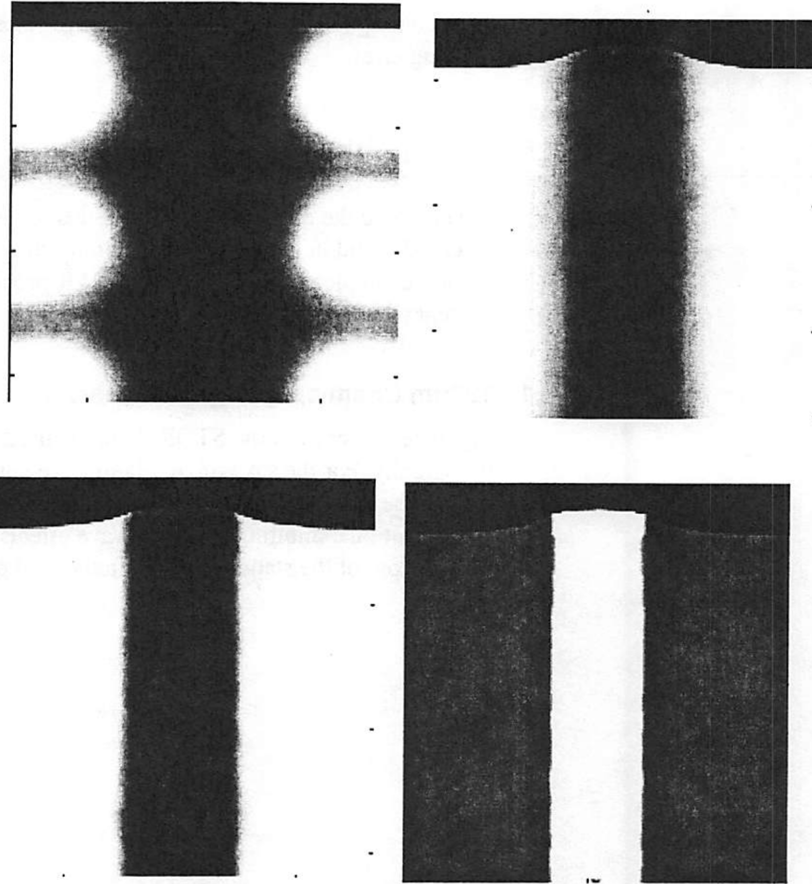

Figure 9. (a) acid concentration before PEB (b) acid concentration after PEB (c) deprotected sites concentration. (d) resist line after wet development

7.5.2 Top surface imaging (TSI)

Fig. 10 demonstrates the feasibility of STORM at simulating the 193nm TSI process. We show the case for the positive tone process. Fig. 10a shows the extent of crosslinking in the resist after exposure. Fig. 10b shows the resist after silylation and Fig. 10c shows the resist line after dry development.

7.5.3 Bilayer resist (BLR)

Fig. 11 shows similar simulation results for the BLR process for 193nm lithography. Fig. 11a shows the resist after exposure and wet development. The top layer is assumed to be a silicon containing resist and the undeveloped line shown in the figure contains silicon. Fig. 11b shows the resist remaining after some intermediate etch time. Note the randomness in the resist feature. This is due to the Monte Carlo simulation of the ion

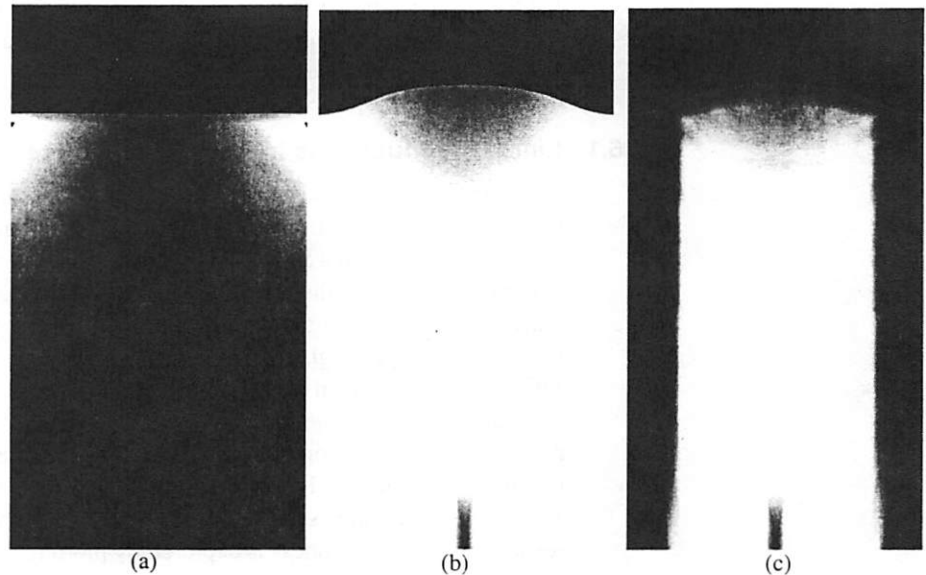

Figure 10. (a) extent of crosslinking after exposure. (b) silylated profile (red region shows silicon concentration) (c) resist feature after dry development.

bombardment and rapid increase in etching rate at bombarded sites. Fig. 11c shows the resist line after dry development

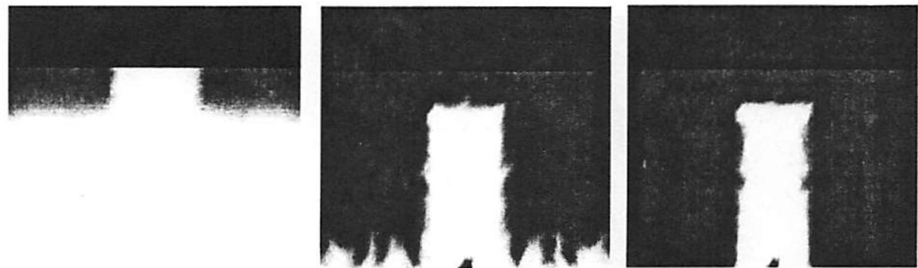

Figure 11. (a) silicon containing resist after wet development. (b) resist remaining after some intermediate etch time. (c) resist feature after dry development.

7.6 193nm lithography technology issues simulation

Line edge roughness (LER) is the most important issue hampering the manufacturability of surface imaged resist processes. STORM is the first simulator known to offer simulation of this important technology issue. Another technology issue of concern is line-

end shortening (LES) effects in CAR. The relative impact of LES effect on smaller features demands that causes of LES be investigated and controlled to allow extension of CAR for deep submicron resist applications. A cost effective way of investigating LES is through simulation and STORM provides the means of simulating LES. The reader interested in our work on LES should consult [34]

7.6.1 Line edge roughness in surface imaged resist processes

The current surface imaged models in STORM assumes that LER is caused by the random nature of the sputtering of the low concentration silicon at the profile edges instead of its conversion into a SiO_x barrier. In other words, when an ion bombards the silicon containing surface in the presence of activated neutrals, the ion bombardment can accelerate the conversion of the silicon to SiO_x or it can sputter the silicon. While silicon areas containing enough silicon content have a high probability of being converted to SiO_x barrier, the silicon concentration at the edges of silylated profile is very sensitive to this randomness of either barrier conversion/silicon sputtering process caused by the random nature of the ion bombardment. By using the above assumptions, we show simulation results for LER in fig. 12. Fig. 12a shows the top view of the silylated resist. Fig. 12b, 12c and 12d shows the roughness after 10 seconds, 15 seconds and 20 seconds respectfully. The roughness is captured by plotting the resist concentration contours after the simulation and choosing a certain concentration value as the threshold value (below this value resist is assumed to be removed, above this value the resist remain)

and measuring the line width variations in the etched resist to obtain roughness information.

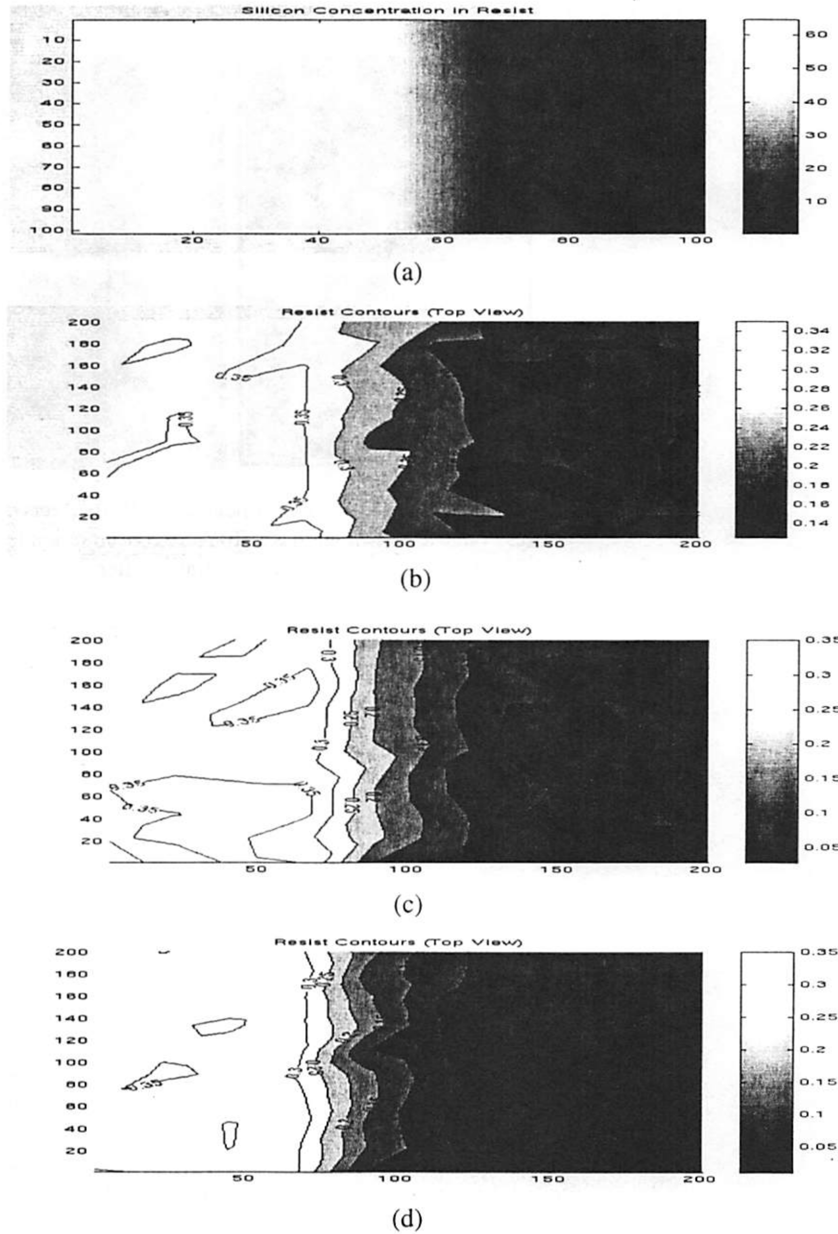

Figure 12. Top view simulation of etched profiles. (a) initial silicon concentration. (b) roughness simulation after 10 seconds (c) roughness simulation after 15 seconds (c) roughness after 20 seconds.

7.6.2 Line-end shortening effects in DUV resist processes

Fig. 13 shows the LER simulation which attempts to quantify the deviation of the final resist feature from the mask feature. Application results show that LES simulation using STORM can predict experimental results to within 10% [34].

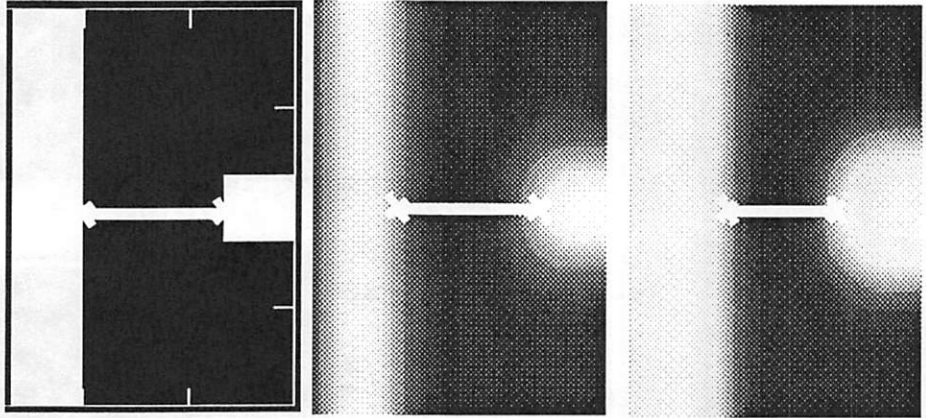

Figure 13. Top view profile simulation of PEB effects on line end shortening in APEX-E (a) Resist line as drawn on mask. (b) Acid concentration in resist after exposure simulation using SPLAT. (c) Activated sites concentration after PEB simulation showing a shorter gap than drawn on mask.

CHAPTER 8

Summary

Rigorous simulation tools for advanced optical lithography resist processes have been developed and named STORM. This name stands for Simulation Tools for Optical Resist Models. STORM's simulation engine is based on advanced numerical methods such as the second order backward difference formula (BDF2) stiff ordinary differential equations (ODE) numerical integrator and the Krylov subspace Newton convergence accelerator. The efficiency of STORM at simulating highly nonlinear model-equations has allowed us to explore more mechanistic based moving boundary models to improve the model prediction of experimental results. The proposed models for wet and dry development process are first pass models and require experimental verification to validate the underlying physical assumptions. STORM simulation of these models allows, for the very first time, deep submicron resist processes such as bilayer resist (BLR), top surface imaging (TSI) and chemically amplified resist (CAR) to be simulated and simulation results are presented in this report. Simulation results of special technology issues in deep submicron lithography such as line-edge roughness (LER) and line-end shortening (LES) are also presented. Typical simulation performance times were under 15 minutes for all the processes except the dry development process. The performance of STORM is degraded during dry development simulation because of the nondeterministic nature of the Monte Carlo method for ion bombardment. Simulation for dry development was under 50 minutes. The simulation tools in STORM can be applied to simulate other process modules besides lithography. STORM program release information can be obtained at the following web site, http://microlab.eecs.berkeley.edu/~ebo.

References

[1] A. R. Neureuther, "Simulation of Semiconductor Lithography and Topography", Monograph in preparation for Springer-Verlag, University of California, Berkeley, 1996.

[2] S. Pantas, "Finite Element Methods for Process Simulation Application to Silicon Oxidation", Ph.D. Thesis, Memorandum No. UCB/ERL M88/26, University of California, Berkeley, May 1988.

[3] M. Zuniga, E. Croffie, and A. Neureuther, Proc. SPIE, Vol. 3333 611-624. (1998)

[4] Dill, F., Neureuther, Tuttle, J and Walker, E. , *IEEE Trans. Electron Devices*, ED-22, No 7 pp.456-464, Sept. 1975.

[5] W. G. Oldham, S. N. Nandgaonkar, A. R. Neureuther, and M. O'Toole, *IEEE Trans. Electron Devices*, ED-26, No 4 pp.717-722, April 1979.

[6] R. Ferguson,

[7] C. Mack, Inside PROLITH: A Comprehensive Guide to Optical Lithography Simulation, Finle Technologies, Inc. (1997).

[8] Hartney, M.A.Journal of Vacuum Science & Technology B, 11(3) 681-7 May/Jun 1993.

[9] Pierrat, C. Journal of Vacuum Science & Technology B, 10(6) (1992) 2581-88.

[10] M. Zuniga, E. Croffie, and A. Neureuther, Proc. SPIE, Vol. 3333 611-624. (1998).

[11] see http://speedie.stanford.edu

[12] J. Pelka, Microelectronic Engineering, 14, pp.269-281 (1991).

[13] see http://www.cs.cmu.edu/~quake/triangle.html

[14] J. Reddy, An introduction to the finite element method, McGraw Hill, New York, (1993).

[15] R. N. Haward and G. Thackray, Proc. Roy. Soc. A., 302: 453-472, 1968.

[16] K. Miller, Lecture Notes for Numerical Solutions of Ordinary Differential Equations (Math 228A), University of California, Berkeley, Fall 1997.

[17] N. Carlson and K. Miller, Design and application of a gradient-weighted Moving Finite Elements, Part 1, Report No. 236, Center Appl Math., Purdue U., May 1994 43-46.

[18] C. W. Gear, Numerical Initial Value Problems in Ordinary Differential Equations.Prentice Hall, Inc, New Jersey pp. 215-220, (1971).

[19] see http://www.cs.berkeley.edu/~xiaoye/superlu.html

[20] G. Wallraff, J. Hutchinson, W. Hinsberg, F. Houle and P. Seidel. Microelectronic Engineering 27 397-400 (1995).

[21] J. Bruce, "APEX PEB evaluation", Feb. 5, 1992, IBM Burlington internal memo

[22] T. Yoshimura, Y Nakayama, and S. Okazaki. J. Vac. Sci. Technol. B Nov/Dec (1992).

[23] . Postnikov, M. Stewart, M. Nierode, D. Medeiros, G. Willson. Private Communications. Aug. (1998).

[24] S. Postnikov, M. Stewart, M. Nierode, D. Medeiros, G. Willson. Private Communications. Aug. (1998).

[25] L. Pain, C. Le Cornec, C. Rosilio, P Piniez, Proc. SPIE, Vol. 2724 100-109 (1996).

[26] J. Crank, The Mathematics of Diffusion, Oxford University Press, New York, (1975).

[27] J. Crank, G.S. Park, Diffusion in Polymers, Academic Press, London, U.K., (1987).

[28] H. Fujita, A. Kishimoto, and K. Matsumoto, Transactions of the Faraday Society, Vol. 56, 424-437 (1960).

[29] Spence.

[30] W. G. Oldham, A.R. Neureuther, Solid State Technoloty, p.106 May 1981.

[31] R. Visser, J. Schellekens, M. Reuhman-Huisken, L Van Ijzendoorn, Proc. SPIE, Vol. 771 111-117 (1987).

[32] B. Roland, R. LomBerts, C. Jakus, and F. Coopmans, Proc. SPIE, Vol. 771 69-76 (1987).

[33] M. A. Lieberman, A. J. Lichtenberg, Principles of Plasma Discharge and Materials Processing, John Wiley & Sons, Inc, New York, (1994).

[34] M. Cheng, E. Croffie, and A. Neureuther, Proc. SPIE, Vol. 3678, (1999).

[35] Kamon, K.; Nakazawa, K.; Yamaguchi, A.; Matsuzawa, N.; Ohfuji, T.; Sasago, M.; Kanzaki, K.; Tagawa, S., Proc. SPIE, vol.3333, p.472-83, 1998

[36] Karafyllidis, I.; Hagouel, P.I.; Neureuther, A.R., Microelectronic Engineering Microelectron. Eng. vol.45, (no.1), Elsevier, Feb. 1999. p.71-84.

[37] Han-Ming Wu; Graves, D.B.; Kilgore, M., Plasma Sources Sci. Technol. , vol.6, (no.2), May 1997. p.231-9.

[38] Kruger, C.H.; Owano, T.G.; Laux, C.O. IEEE Trans. Plasma Sci. , vol.25, (no.5), IEEE, Oct. 1997. p.1042-51.

[39] see http://math.berkeley.edu/~sethian/level_set.html

[40] see http://www.sigma-c.de